Supporting Information

Electrochemical Dinitrogen to Ammonia Reduction at a Nickel(II) Site: An Easy Access to an Air-Stable Catalyst

Jayasree Kumar, Nikhil George Mohan, Tamilselvi Gurusamy, Sai Manoj N. V. T. Gorantla, Prathap Ravichandran, Kartik Chandra Mondal*, Kothandaraman Ramanujam*

Department of Chemistry, Indian Institute of Technology Madras, Chennai- 600 036, India.

Contents:

1. General Information

The chemical substances, such as Nickel chloride hexahydrate ($NiCl_2 \cdot 6H_2O$), Triethyl amine (Et_3N), and phenol from Fischer Scientific, were purchased from available commercial sources. Ortho-vanillin, 2-Aminophenol, Methanol, THF from SRL, and Tetra-butyl ammonium hexafluorophosphate (n-Bu_4NPF_6) from Sigma Aldrich. All the materials were used as received. The solvent methanol was steam distilled and stored under 3 Å molecular sieves before use. All the reactions are carried out in an open atmosphere at ambient temperature.

2. Synthetic Procedures:

The reported Schiff base ligand H_2LMe is a condensed product obtained from a combined equimolar mixture of o-vanillin and 2-amino 4-methyl phenol in hot methanol following a similar procedure.[S1]

2.1. Synthesis of a catalyst $[Ni_4(L\text{-}Me)_4(EtOH)_4]$ 1:

An equimolar mixture of H_2L-Me (10 mmol) and $NiCl_2 \cdot H_2O$ (10 mmol) was placed in a 250 mL conical flask, and 125 mL MeOH was added at room temperature in air. The mixture was stirred for ten min. to obtain a clear orange solution. Triethyl amine (Et_3N) (20 mmol) was dropwise added to get a clear greenish-brown solution, which was stirred only for another 20 min to obtain a greenish-orange crystalline precipitate of $[Ni_4(L\text{-}Me)_4(MeOH)_4]$ in 95-97% yield. The crude product was washed using cold methanol (2x10 mL) to remove Et_3N/Et_3N.HCl. The solid was dried at 60 °C for 2-3 h and applied under a vacuum for 3 h. A portion of the compound was dissolved in dry THF and diffused with dry ethanol, which produced black blocks of X-ray quality crystals of $[Ni_4(L\text{-}Me)_4(S)_4]$ (S = EtOH; **1**) on the next day. Before being subjected to electrochemical studies and characterisation techniques, each batch underwent a similar drying and vacuum treatment. Ni(II) is known to labile complexes, and hence, the coordinated solvent molecules can be easily replaced by other solvents during recrystallisation. *m/z* = 1253; $[M + H]^+$; M = $(L\text{-}Me)_4Ni_4$.[S1] $[Ni_4(L\text{-}Me)_4(EtOH)_4]$ **1** is susceptible to loss of coordinated EtOH if stored in the air. UV/Vis and IR spectra of **1** were shown in (Figures S9 and S15) respectively. Those lost EtOH are replaced by water molecules from moisture. Hence, $[Ni_4(L\text{-}Me)_4(EtOH)_4]$ **1** are stored under a dinitrogen-filled Schlenk flask.

Important notes: Storing the MeCN solution of **1** in the open air for two weeks and subjecting it to mass spectrometric analysis have shown that **1** displays oligomerisation (n = 1, 2, 4, 5; Scheme S1). Tetramer and pentamers are observed to bind with aerial N_2, which has been confirmed by ESI-MS measurements of the diluted solution of this stock solution (Figure S1). Our additional experimental observations have been summarised in (Scheme S1).

Complex $[Ni_4(L\text{-}Me)_4(DMF)_4]\cdot DMF$[S1]: The powdered sample of **1** was dissolved in a minimum amount of DMF and placed under slow evaporation to obtain green blocks of $[Ni_4(L\text{-}Me)_4(DMF)_4]$.

3. ESI-MS measurements:

High-resolution mass analysis was carried out using Agilent Technologies 6545 Q-TOF LC/MS equipped with an electrospray mode of 'TOF Analyzer' spectrometer at the Department of Chemistry, IIT Madras, India. The full profile data obtained from **1** successfully matched the experimental isotopic pattern with the theoretical pattern corresponding to an empirical formula using the mMass software package.[S1]

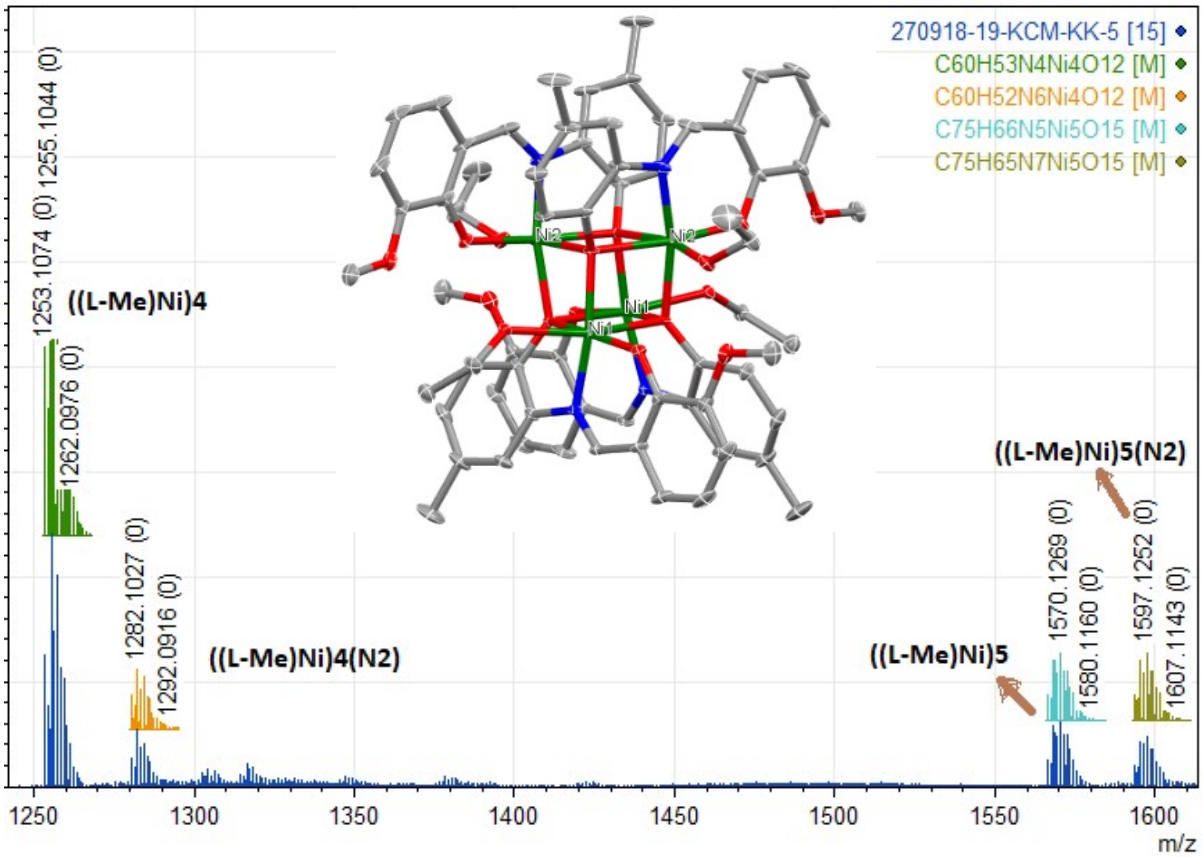

Figure S1 Experimental (blue, bottom) and simulated (green, orange, bluish green and yellowish green, top) ESI-MS spectra of the tetramer, pentamer and their dinitrogen bonded species $[(L\text{-}Me)_4Ni_4 + H]^+$, $[(L\text{-}Me)_4Ni_4(N_2)]^+$ (left) and $[(L\text{-}Me)_5Ni_5 + H]^+$, [(L-

$Me)_5Ni_5(N_2)]^+$ (right). Molecular Structure of tetrameric complex **1** $[((L\text{-}Me)Ni)_4(Sol)_4]$ (Inset).

1 (0.2 mmol) was dissolved in 25 mL of dry THF, resulting in orange coloured solution, then added KC_8 (0.8 mmol) led to a dark brown solution that was instantly taken out of the glove box to continue stirring for 3 h under N_2 flow in the Schlenk line. This solution was diluted with MeCN to micromolar concentration to perform ESI-MS measurements. The well-matching of pattern and their values between the simulated and experimental plots (Figure 4) suggests the formation of dinitrogen bonded dimeric species of $[\{(L\text{-}Me)Ni(N_2H)\}_2 + Na]^+$ (left) and $[\{(L\text{-}Me)Ni(N_2H)\}_2 + 3Na]^+$ (right) in solution phase.

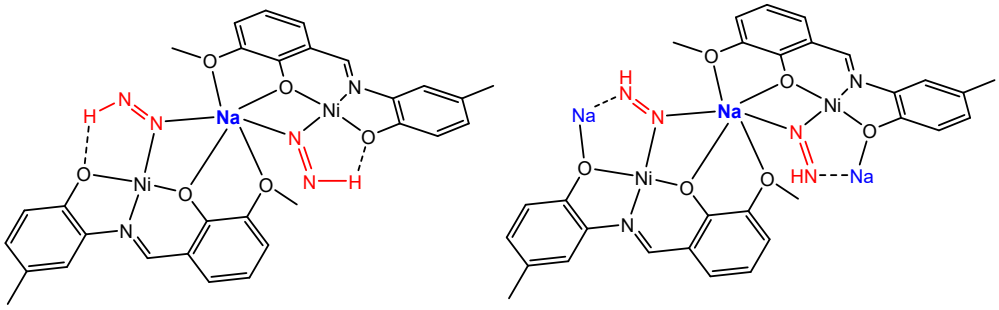

Figure S2 ESI-MS characterized dinitrogen bonded dimeric species of $[\{(L\text{-}Me)Ni(N_2H)\}_2 + Na]^+$ $[(\mathbf{3})_2 + \mathbf{Na}]^+$ (left) and $[\{(L\text{-}Me)Ni(N_2H)\}_2 + 3Na]^+$ $[(\mathbf{3})_2 + \mathbf{3Na}]^+$ (right).

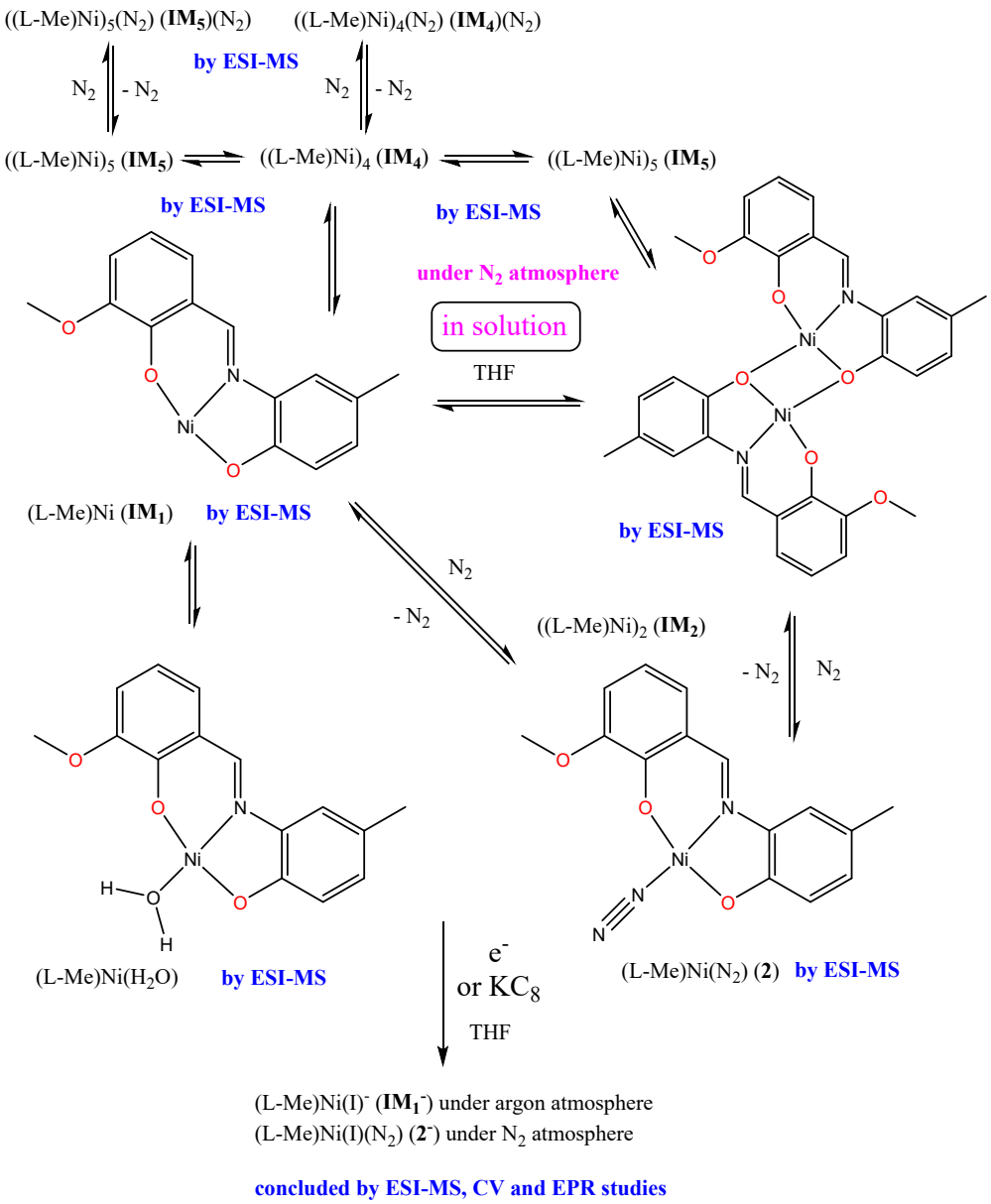

Scheme S1 The solution dynamics/oligomerisation, N_2-binding and reduction of **1**.

4. EPR Analysis:

The EPR measurements were recorded at X-band (8.75-9.65 GHz) using a JEOL JES FA 200 spectrometer at 77K. Complex 1 (0.2 mmol, 250 mg) and KC_8 (0.8 mmol, 110 mg) were inside the glove box in an oven-dried Schlenk flask, and 30 mL of dry THF was added. The mixture started stirring continuously for 4 h under purging of N_2 and Ar gas separately, fitted with the Schlenk line setup. Again, using the glove box facility, both the dark brown coloured filtrates were transferred to the two individual quartz capillary tubes whose mouths were adequately greased, which were then placed inside the quartz EPR tubes to carry out the experiment. (microwave power: 1 mW, modulation amplitude: 0.1 mT).

(a)

(**1**) in THF

$4\ KC_8$

THF, rt

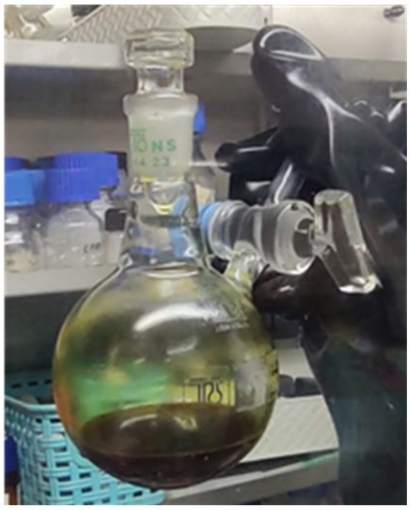

(L-Me)Ni(I)$^-$ (**IM$_1^-$**) under Ar atmosphere
(L-Me)Ni(I)(N_2) (**2$^-$**) under N_2 atmosphere

concluded by ESI-MS, CV and EPR studies

(b)

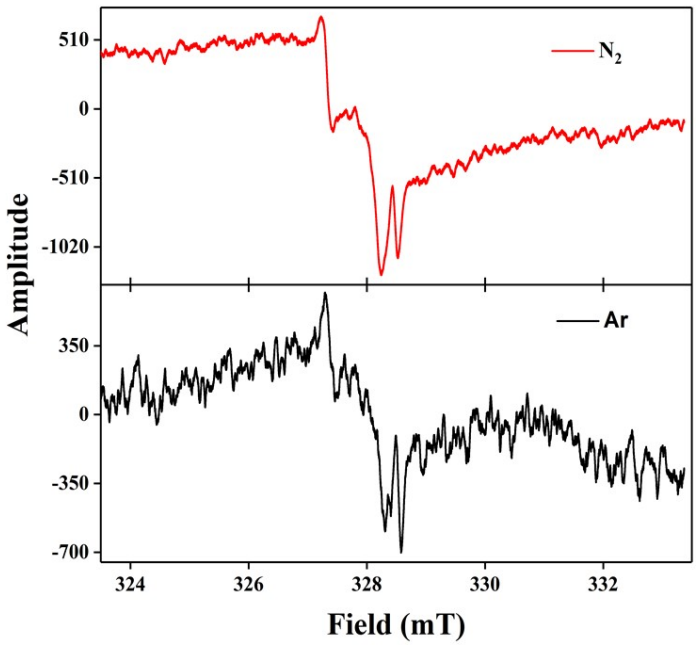

Figure S3 (a) Reaction of ((L-Me)Ni)$_4$ (**1 - 4Sol**) with KC_8 in the molar ratio (1:4) in dry THF (above) (b) Solution EPR spectra of [(L-Me)Ni(I)]$^-$ (**IM$_1^-$**) under N_2 and argon.at 77 K (below). X-band EPR measurements have confirmed the Ni(I) intermediate formation.[S2]

The EPR resonances of **IM$_1^-$** are similar to the EPR spectrum for a nitrogen-bonded Ni(I) complex reported[S2] by Pfirrmann *et al*.

Started with the optimized geometry of [(L-Me)Ni]$^-$ (**IM$_1^-$**)/[(L-Me)Ni(N_2)]$^-$ (**2$^-$**) at the BP86/def2-TZVPP level of theory. Utilising ORCA 5.0.2 version, g-factors are calculated at the level of SA-CASSCF+NEVPT2-SC/DKH-def2-TZVPP level of theory with active space

(9,5), i.e., nine electrons in five 3d-orbitals. Simulated g-tensors are g_{xx} = 2.028, g_{yy} = 2.101, g_{zz} = 2.226.

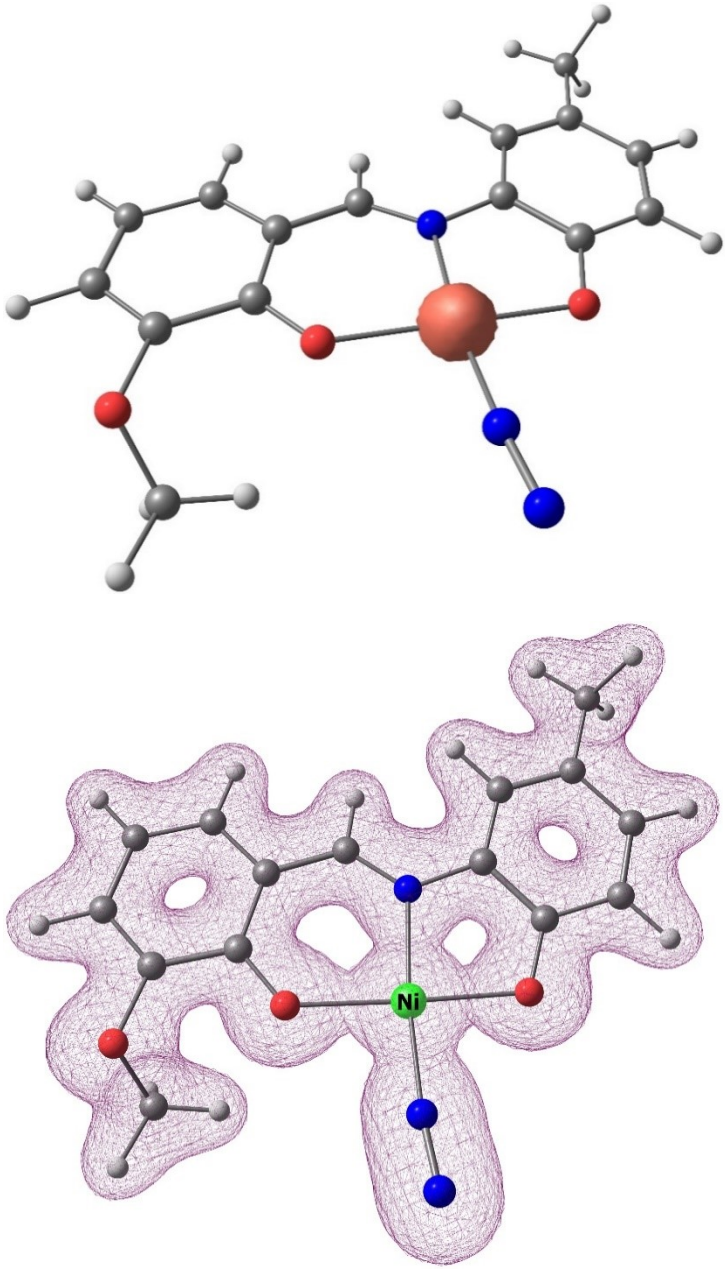

Figure S4 (a) Spin density around Ni(I) centre (above). (b) The distribution of the electron densities in $[(L\text{-}Me)Ni(N_2)]^-$ (**2**$^-$) (below). Active space (m, n) where m is the number of electrons and n denotes the orbitals (m = 9; n = 5).

5. Structure determination:

Single Crystal X-ray diffraction:

Single crystals were taken, immersed in perfluorinated polyether oil, and placed on a glass slide. Using a polarising microscope, a suitable single crystal was selected and picked up with the help of an appropriate loop. The sample was placed on the tip of the Mitegen MicroMounts equipped with a goniometer head of the instrument. Single crystal data were collected on a Bruker AXS kappa Apex 2 CCD diffractometer,[S3] with graphite monochromatic Mo-Kα radiation (λ = 0.71073 Å) at 293 K. The raw data was integrated by applying required corrections using SAINT PLUS[S4], and absorption correction was carried out using the multi-scan method (SADABS).[S5] The structure was solved using the direct method (SHELXS-97) and refined on F^2 using the full-matrix least-square technique with the shelXL-2018/3 program and WinGX v1.70.01[S6-S8] program packages. Anisotropic displacement parameters were applied for all non-hydrogen atoms.

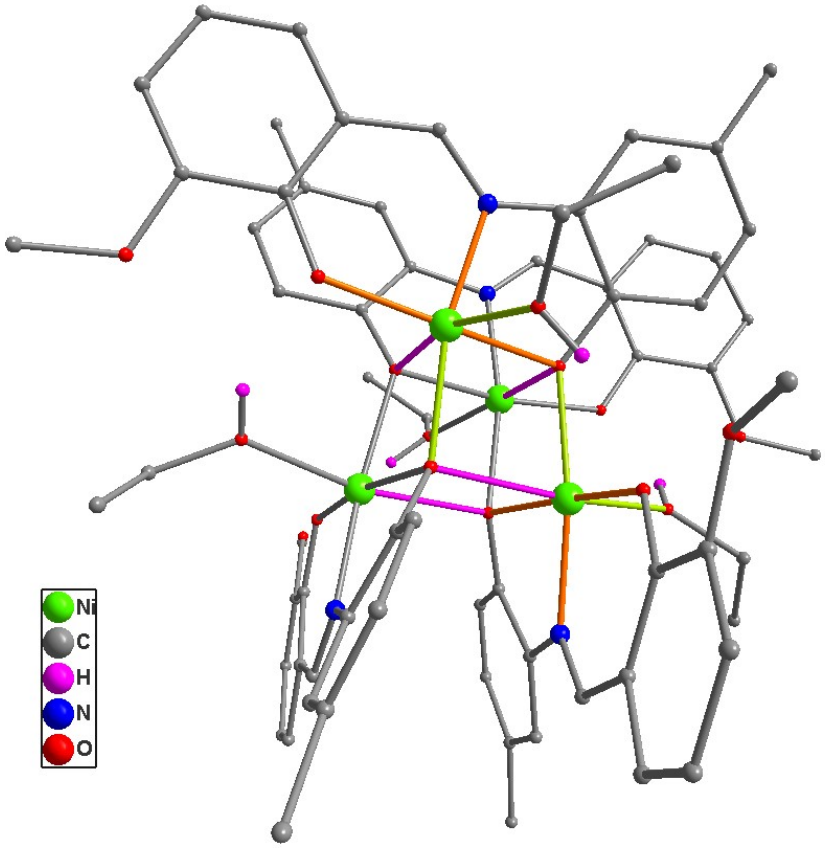

Figure S5 The molecular structure of **1**. Selected orange Ni-O/N bond distances are 1.96/1.983 to 2.057/2.049 Å; The green-coloured Ni-O/N bond distances are 2.053/2.057 to 2.093/2.129 Å. The Ni-O bond is opposite to the Ni-OEtOH bond and is significantly elongated (2.228/2.211 Å, pink in colour. These elongated Ni-O bonds are likely to be weaker and could open up in the solution, displaying oligomerisation.

Compound **1** crystallises in an orthorhombic system with the $C222_1$ space group. The molecular structure of **1** possesses four Ni(II) ions, four L-Me^{2-} and four coordinating ethanol solvent molecules. The orientation of two ligands is perpendicular to the other two. Four Ni-O bonds appear shorter than the other two, which have nearly S_4 symmetry. To bring about the Ni_4O_4 cubane, all four symmetry-related Ni(II) ions are bridged by μ_3-O atoms. Each Ni(II) ion is hexacoordinated, where three oxygen atoms are contributed from the imine part of the Schiff base, one from the mono-dentated ethanol, another from the phenolate oxygen of ortho-vanillin part, and the imine nitrogen of the ligand. The Ni(II) and μ_3-O atoms from the amino phenol part of the ligand occupy the alternate vertices of distorted cubane in such a way that two tetrahedral units interpenetrate on one another, where one consists of metal ions, and another made up of μ_3-O atoms. The six faces of distorted cubane are inequivalent to each other. The four lateral faces of the cube parallel to the c-axis are found to be 93.66° and 99.48°, whereas the perpendicular faces show 99.48° and 100.35° respectively. Ni-O-Ni bond angles of the cubane core containing oxygen atoms differed from 90° and diversified widely in the range of 93 to 100°. The ONO donors of Schiff base ligand coordinated Ni^{2+} in a distorted octahedral environment. Six distinct Ni-O bond distances are visible for the oxygen-consisting hetero-cubane core. Those Ni-O bond distances vary in the range between 2.047 and 2.225 Å. At the same time, the O-donor of the ortho vanillin part constitutes Ni-O bond distances of 1.964 Å and 1.968 Å, respectively. The loosely bound coordinated ethanol molecules leave and initiate N_2 binding by ensuring a vacant site. Single crystal X-ray analysis reveals that one methanol and one THF molecule are present in the unit cell lattice.

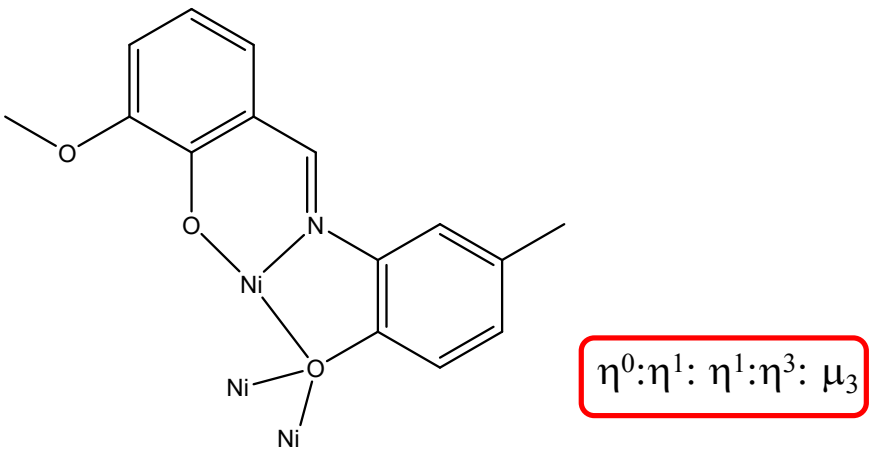

Figure S6 Various bridging modes of Schiff base ligand in Ni_4 **1** complex.

Table S1 Crystal refinement details of $[Ni_4(L\text{-}Me)_4(HOEt)_4]\cdot THF\cdot MeOH$ **1**.

CCDC number **2145462.**

Crystallographic parameters	Crystallographic data
Empirical formula	$C_{73}H_{88}N_4Ni_4O_{18}$
Formula weight	1544.31
Crystal size	0.300 x 0.250 x 0.200 mm^3
Crystal system	Orthorhombic
Space group	$C222_1$
a[Å]	11.8537(3)
b[Å]	27.7370(6)
c [Å]	22.5414(4)
α[°]	90
β[°]	90
γ[°]	90
V[$Å^3$]	7411.3(3) $Å^3$
Z	4
Temperature	200(2) K
ρ[Mgm^{-3}]	1.384 Mg/m^3
μ[mm^{-1}]	1.071 mm^{-1}
F(000)	3240
θ-area[°]	3.2-25.9
Total number of reflections	123783
Unique reflections	7286
R_{int}	0.0946
Number of restraints	90
Parameters	483
$R_1[I>2\sigma(I)]$	0.0398
$wR_2[I>2\sigma(I)]$	0.0974
R_1 [all data]	0.0551
wR_2 [all data]	0.1086
GooF	1.115
Extinction coefficient	n/a
Largest diff. peak/hole max./min.[$e\cdot Å^{-3}$]	0.403 /-0.307 $e.Å^{-3}$

Table S2 Selected bond lengths [Å] and bond angles [°] for **1**.

Ni1-O(2)	1.967(4)	Ni1-N1	1.985(4)
Ni1-O(4)	2.048(3)	Ni1-O(5)#1	2.056(3)
Ni1-O(3)	2.130(4)	Ni1-O(4)#1	2.211(3)
Ni(2)-O(7)	1.963(4)	Ni(2)-N(2)	1.986(5)
Ni(2)-O(4)	2.053(4)	Ni(2)-O(5)	2.056(4)
Ni(2)-O(6)	2.092(4)	Ni(2)-O(5)#1	2.228(4)
O(2)-Ni1-N1	93.00(18)	O(2)-Ni1-O(4)	168.56(14)
N1-Ni1-O(4)	82.84(17)	O(2)-Ni1-O(5)#1	99.52(16)
N1-Ni1-O(5)#1	167.49(17)	O(4)-Ni1-O(5)#1	84.84(14)
O(2)-Ni1-O(3)	103.67(15)	N1-Ni1-O(3)	88.98(18)
O(4)-Ni1-O(3)	86.96(14)	O(5)#1-Ni1-O(3)	88.20(15)
O(2)-Ni1-O(4)#1	90.47(14)	N1-Ni1-O(4)#1	97.88(17)
O(4)-Ni1-O(4)#1	79.62(14)	O(5)#1-Ni1-O(4)#1	81.98(13)
O(3)-Ni1-O(4)#1	163.99(14)	O(7)-Ni(2)-N(2)	94.4(2)
O(7)-Ni(2)-O(4)	97.67(16)	N(2)-Ni(2)-O(4)	167.8(2)
O(7)-Ni(2)-O(5)	170.58(17)	N(2)-Ni(2)-O(5)	81.9(2)
O(4)-Ni(2)-O(5)	85.96(13)	O(7)-Ni(2)-O(6)	100.96(18)
N(2)-Ni(2)-O(6)	88.8(2)	O(4)-Ni(2)-O(6)	90.29(17)
O(5)-Ni(2)-O(6)	87.67(16)	O(7)-Ni(2)-O(5)#1	91.56(15)
N(2)-Ni(2)-O(5)#1	97.8(2)	O(4)-Ni(2)-O(5)#1	80.46(13)
O(5)-Ni(2)-O(5)#1	80.43(13)	O(6)-Ni(2)-O(5)#1	165.36(15)
C(7)-N1-C(6)	125.0(5)	C(7)-N1-Ni1	125.0(4)
C(6)-N1-Ni1	109.7(4)	C(22)-N(2)-C(23)	125.3(6)
C(22)-N(2)-Ni(2)	124.0(5)	C(23)-N(2)-Ni(2)	110.7(4)
C(12)-O1-C(14)	117.6(7)	C(13)-O(2)-Ni1	125.0(4)
C(33)-O(3)-Ni1	132.7(4)	C(33)-O(3)-H(3A)	109.5
Ni1-O(3)-H(3A)	117.3	C1-O(4)-Ni1	107.0(3)
C1-O(4)-Ni(2)	137.4(3)	Ni1-O(4)-Ni(2)	99.56(15)
C1-O(4)-Ni1#1	114.1(3)	Ni1-O(4)-Ni1#1	100.33(14)
Ni(2)-O(4)-Ni1#1	92.54(13)	C(28)-O(5)-Ni**1**#1	137.2(3)
C(28)-O(5)-Ni(2)	108.4(4)	Ni1#1-O(5)-Ni(2)	97.15(14)
C(28)-O(5)-Ni(2)#1	114.4(3)	Ni1#1-O(5)-Ni(2)#1	93.84(14)
Ni(2)-O(5)-Ni(2)#1	99.54(13)	C(31)-O(6)-Ni(2)	131.6(5)

Symmetry transformations used to generate equivalent atoms:

#1 -x+1,y,-z+3/2 #2 x,-y+1,-z+1

6. X-ray Photoelectron Spectroscopy (XPS):

The core level photo-emission analysis was performed using an X-ray photoelectron Spectrometer: Thermo Scientific Nexsa equipped with an Al Kα X-ray source (hν = 1486.6 eV; spot size 10-400 mm). Figure S7a represents the survey spectrum of **1,** showing XPS signals corresponding to C 1s, N 1s, O 1s, Ni (2s, 2p, 3s, 3p), and Ni LMM offering a comprehensive overview of the chemical constituents of **1**.

In Figure S7b, the C 1s spectrum was deconvoluted into four distinct peaks. C=C and C-C are confirmed by the peaks centred at the binding energies of 284.2 eV and 284.7 eV, respectively. This observation suggests that sp^2 and sp^3 hybridised carbon atoms coexist in **1**.[S9-S10] The presence of the peak at around 285.2 eV in C 1s was identified for the C=N conjugate bond[S9], which causes the C 1s peak to broaden and appear somewhat asymmetric.[S9] Furthermore, the deconvoluted C 1s spectrum reveals the presence of C-O (~287.3 eV).[S9]

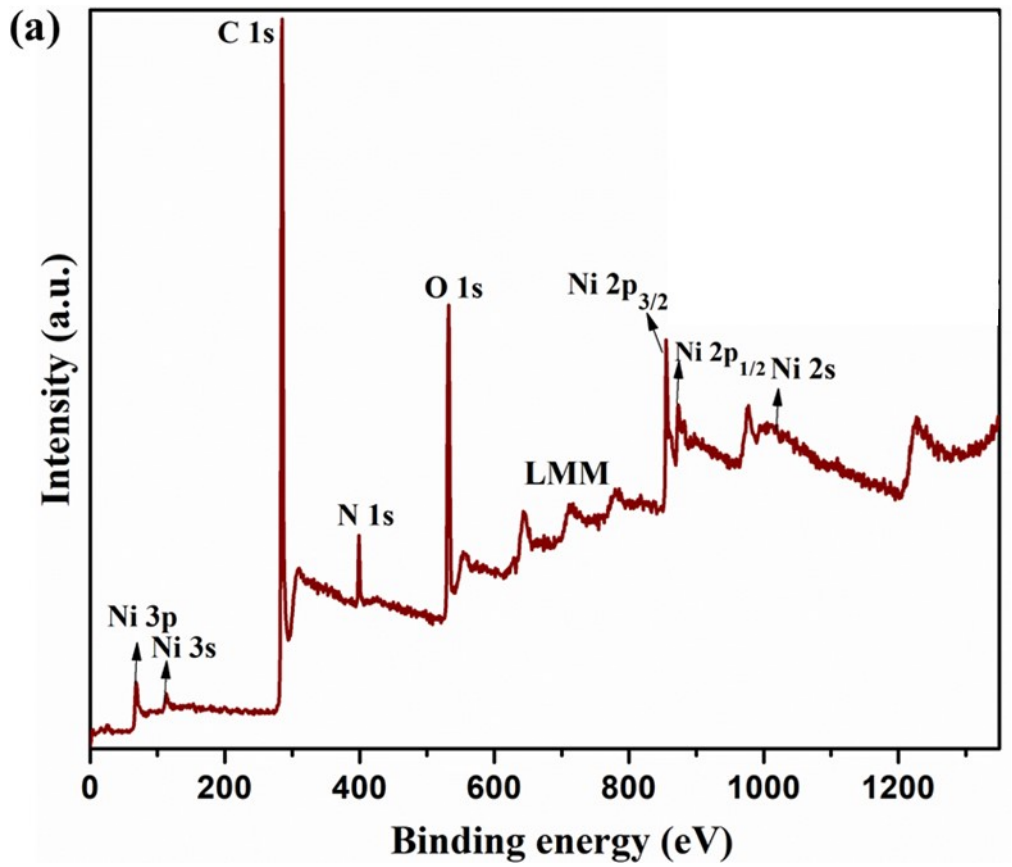

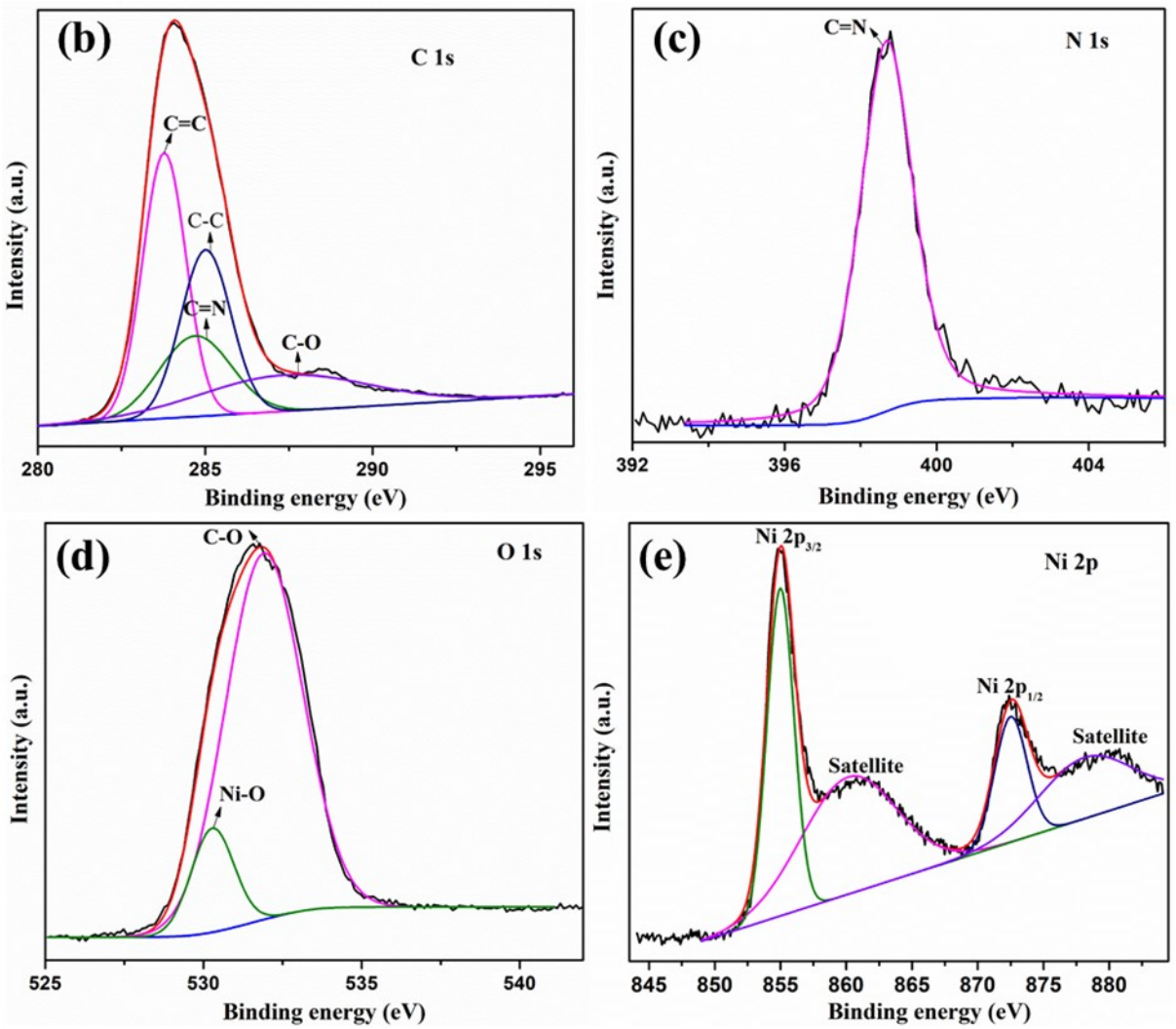

Figure S7 XPS spectra of **1** (a) survey spectrum, (b) C 1s, (c) N 1s, (d) O 1s, and (e) Ni 2p.

In Figure S7c, the appearance of a peak in N 1s at *ca*. 399 eV confirms the existence of the C=N group[S9] in **1,** which is in corroboration with C 1s data. Figure S7d exhibits a high-resolution O 1s spectrum, featuring a peak at around 532 eV, matching with the reported value of the C-O group.[S11] Moreover, the O 1s profile reveals a peak at ~ 530 eV, indicative of the presence of the Ni-O group.[S12] Figure S7e shows the Ni 2p peak corresponding to Ni^{2+} in **1,** along with satellite peaks (860.17 and 878.15 eV).[S13] Two sharp peaks at 854.99 eV and 872.5 eV indicate the characteristic spin-orbit doublets, $2p_{3/2}$ and $2p_{1/2}$.[S10, S14] The molecular structure of **1** represented in Figure S5 displays the Ni_4O_4 cubane structure with the hexa-coordination for all four Ni ions. Integration of Ni 2p and N 1s peaks (12786.2 and 12674.9) indicates the ratio of Ni to N is ~ 1, which conforms with the molecular formula of **1**.

7. SEM Analysis:

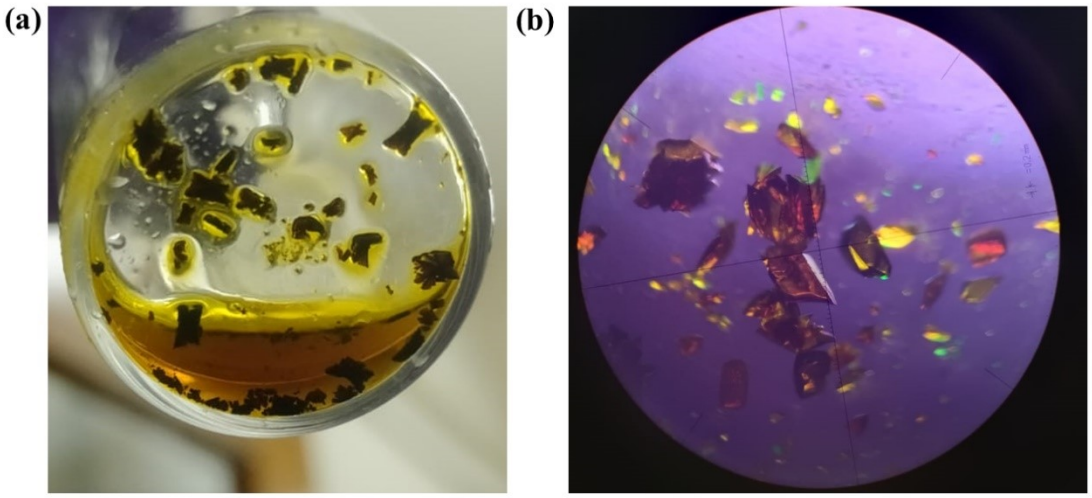

Figure S8 (a) The image displays the crystal blocks of **1**, $[Ni_4(LMe)_4(HOEt)_4]$, which were obtained from the gradual diffusion of EtOH with THF solution. (b) Crystals of **1** under an optical microscope with polarised light.

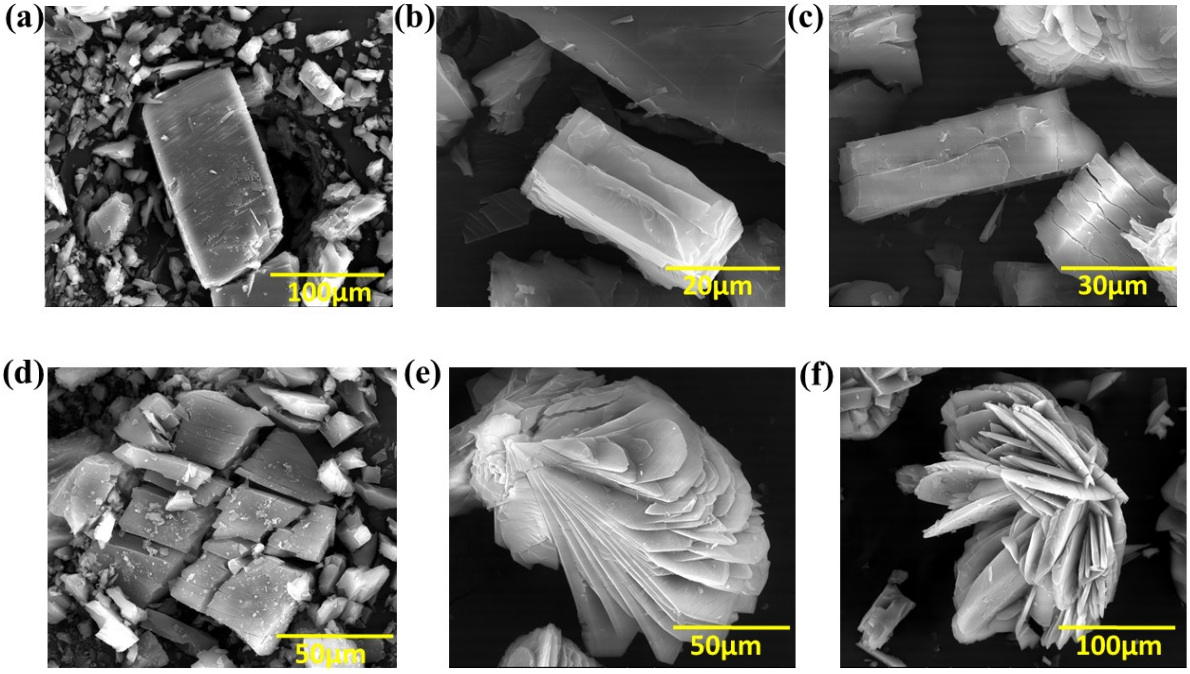

Figure S9 FE-SEM pictures from (a) to (f) illustrate the block-like nature of the crystals of **1** formed through the crystallisation process involving THF and EtOH.

Freshly prepared **1** was subjected to SEM analysis. The high-resolution microscope equipped with a Field Emission Gun (FEG) assembly featuring a Schottky emitter (from -200V to 30kV) was used as the source. The block-like crystal of compound **1** was observed (Figure S9 a-c). These crystals were used for the SC-XRD measurement.

8. Raman Studies:

Raman spectra were collected in the region from 50-4000 cm^{-1} on a BRUKER RFS 27-stand-alone unit spectrometer equipped with the FT-Raman microscope (RamanScopeIII) containing a room-temperature InGaAs detector. A fully software-controlled 1064 nm line of continuous wave (CW) generating Nd: YAG laser sample excitation source was used. The slit allows the spectral resolution of 2 or 4 cm^{-1}. **1** was continuously subjected to vacuum and Ar purging alternatively at 100 ˚C under an oil bath. Post-treated **1** (0.27 mmol, 337 mg) in 25 mL of dry toluene was allowed to stir until a partially dissolved orange-coloured solution was obtained with some undissolved compound left behind at the bottom kept inside a -40 ˚C fridge for 1 h. Under cold conditions, KC_8 (1 mmol, 135.2 mg) was added to the slurry and stirred for 24 h in an N_2-saturated environment. The obtained brown-coloured content was filtered under N_2, and the clear orange solution was evaporated to dryness under a vacuum. The resulting orange compound (IM1−) was grounded with a KBr (≥99.0%, from Sigma Aldrich) and transferred into the metal grooves to get it analysed from solid-state Raman spectroscopy. Likewise, **1** was allowed to undergo similar treatment under Ar atmosphere, and the obtained ($\mathbf{2}^-$) data were also analysed for a better comparison.

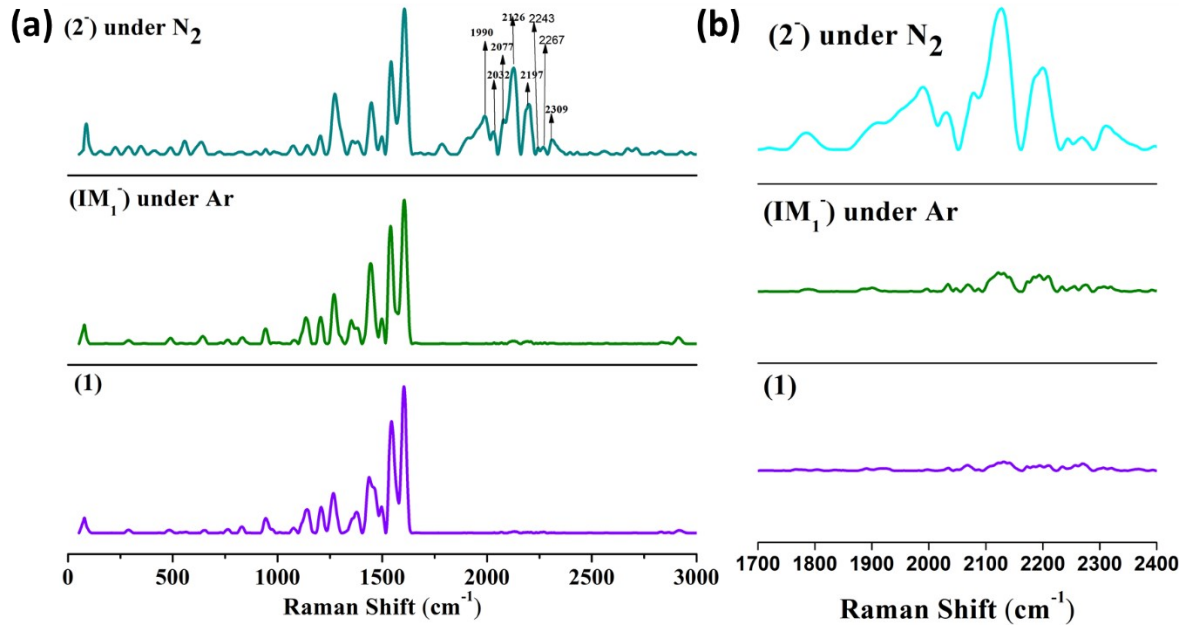

Figure S10 (a) Comparison of solid-state Raman spectra of **1, 1** under Ar and **1** under N_2. (b) Magnified spectra of the region ascribed to N_2 binding.

9. Attenuated total reflectance (ATR):

Solution ATR spectra were recorded for blank toluene and the solution mixtures $[(L\text{-}Me)Ni]^-$ ($\mathbf{IM_1}^-$) and $[(L\text{-}Me)Ni(N_2)]^-$ ($\mathbf{2}^-$), respectively. Bruker-Alpha Eco-ATR FTIR instrument equipped with a versatile ZnSe ATR crystal providing high throughput was utilised. Solution samples of ($\mathbf{IM_1}^-$), ($\mathbf{2}^-$), and dry THF alone were taken in separate vials and allowed to freeze under liquid N_2 until frozen. As soon as it started liquefying, the analytes were taken and injected between the NaCl plates and placed in a clean, demountable solution cell holding. The IR spectra were collected at room temperature, and the frequencies were reported in cm^{-1}.

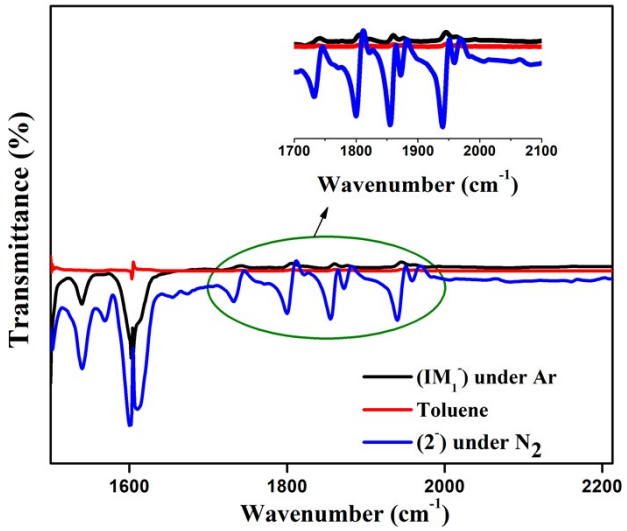

Figure S11 ATR-IR spectra of complex **1**, intermediates $(\mathbf{IM_1})^-$, and ($\mathbf{2}^-$).

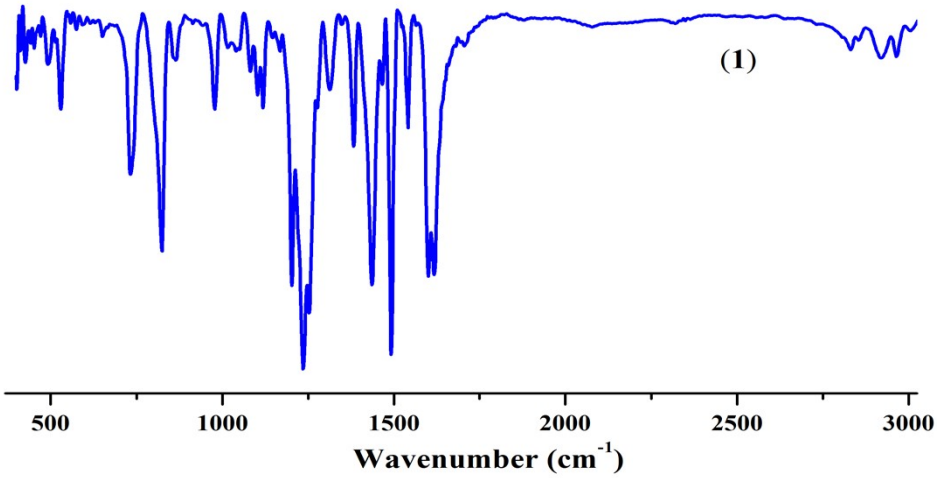

Figure S12 IR spectrum of complex **1**.

10. Structural Stability of 1:

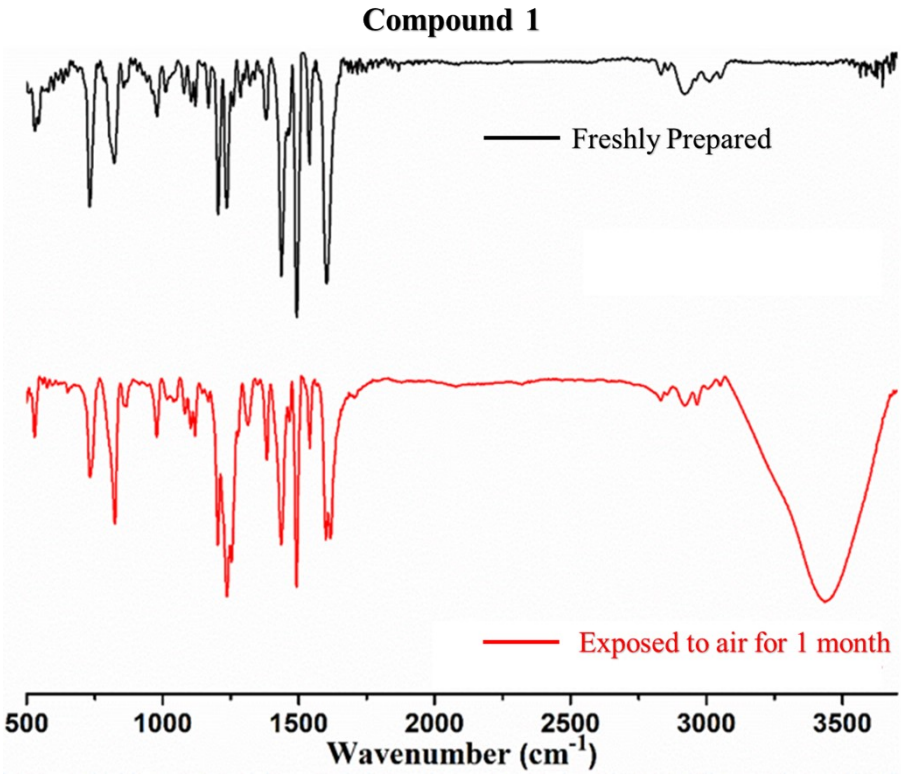

Figure S13 Comparison of FT-IR spectra of compound **1**: freshly synthesised (black, top) and exposed to ambient conditions (red, bottom) for one month.

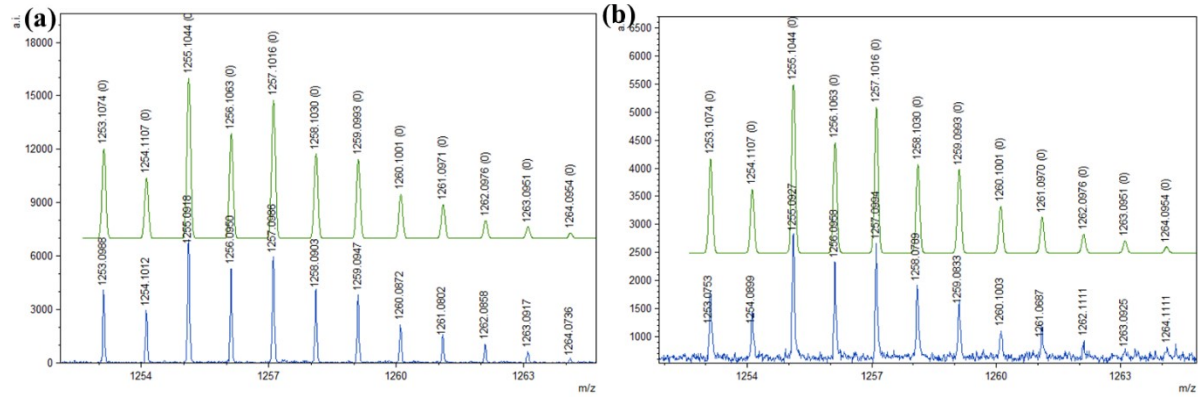

Figure S14 (a) Experimental (bottom, blue) and simulated (green, top) ESI-MS spectra of freshly prepared **1** and (b) Experimental (bottom, blue) and simulated (green, top) ESI-MS spectra of **1** after atmospheric exposure for a month.

11. Electrochemical studies:

Complex $[Ni_4(L\text{-}Me)_4(Sol)_4]\cdot THF\cdot MeOH$ **1** was heated at 100 ºC under an applied vacuum to remove the solvent, and the mass obtained is $(L\text{-}Me)_4Ni_4$ (**1 - 4Sol**) (Confirmed by ESI-MS and TGA analysis)[S1] which was subjected to all electrochemical measurements.

Electrochemical measurements:

All the measurements have been reported concerning Fc^+/Fc. For NRR-related experiments, a potentiostat test was conducted in an N_2-saturated THF solution with a continuous flow of pure

N_2 (99.999% purity) into the cathodic compartment. The N_2 gas was purged through an aqueous solution for 2.5 h (more than the duration (i.e. 5000s) employed in our chronoamperometry measurement-based data reported in Figure 7b). We subjected it to the IC analysis to detect the presence of any nitrogen oxide species using the Metrohm-A Supp 5 250/4.0 column. We have used $NaNO_2$ and KNO_3 (1 ppb to 10 ppm) solutions as standards for nitrite and nitrate, respectively. In addition to the above, 2 mL of the solution was pipetted out and tested for ammonia using the indophenol method. The corresponding IC curves and the UV-Vis plot are given in Figure S15a and Figure S15b, respectively. IC measurements indicate the presence of 20 ppb of NO_2^- in the solution, corresponding to the amount of NO in the feed gas. No NO_3^- was detected within the solution. From these figures, it is apparent that even if the entire amount of NO_x is assumed to react to form ammonia, then the amount produced would be around 20 ppb. Also, the ammonia detected in the feed gas is about 86 ng. Even assuming the worst-case scenario where the amount of ammonia detected is because of the contaminants, the ammonia yield observed post-electrolysis is much higher than the amount of contaminants in the solution.

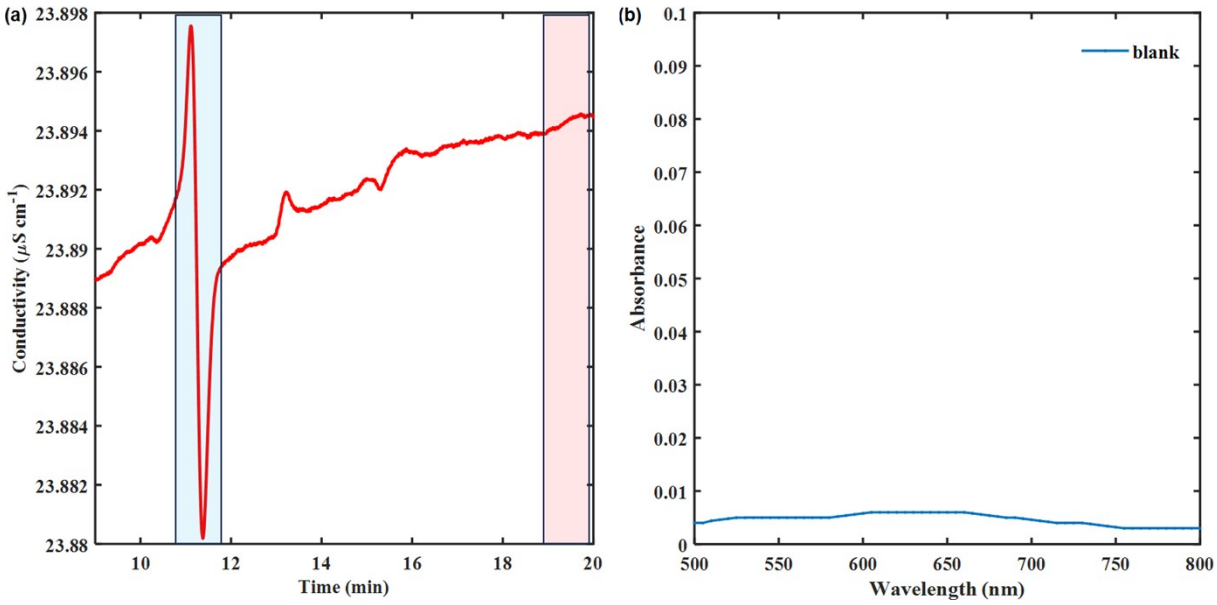

Figure S15 (a) Ion Chromatogram of the aqueous solution through which N_2 gas was purged for 2 h and (b) the UV-Vis absorption of the indophenol dye showing a maximum at 650 nm used for the quantification of ammonia in the feed gas.

We must avoid the large availability of protons around the electrode to suppress the competing HER reaction (especially at high reduction potentials). To limit the availability of protons, we have adopted a non-aqueous electrolyte (tetrahydrofuran) with a limited supply of external proton source, phenol. Thus suppressing the competing HER.

Any protic source in place of phenol can assist in the reduction of N_2. To strengthen our argument, we have demonstrated ammonia production using ethanol as the proton source, which is much cheaper than phenol. Here, we can also obtain ammonia after 2 h of chronoamperometry at -2.3 V vs Fc/Fc^+; however, the yield differs from the yield observed when using a proton source. This is because the rate of the competing HER process and the proton-coupled electron transfer process in the NRR is affected by the change of the proton source. Figure S16 indicates the UV-Vis spectrum obtained using ethanol as a proton donor post-electrolysis.

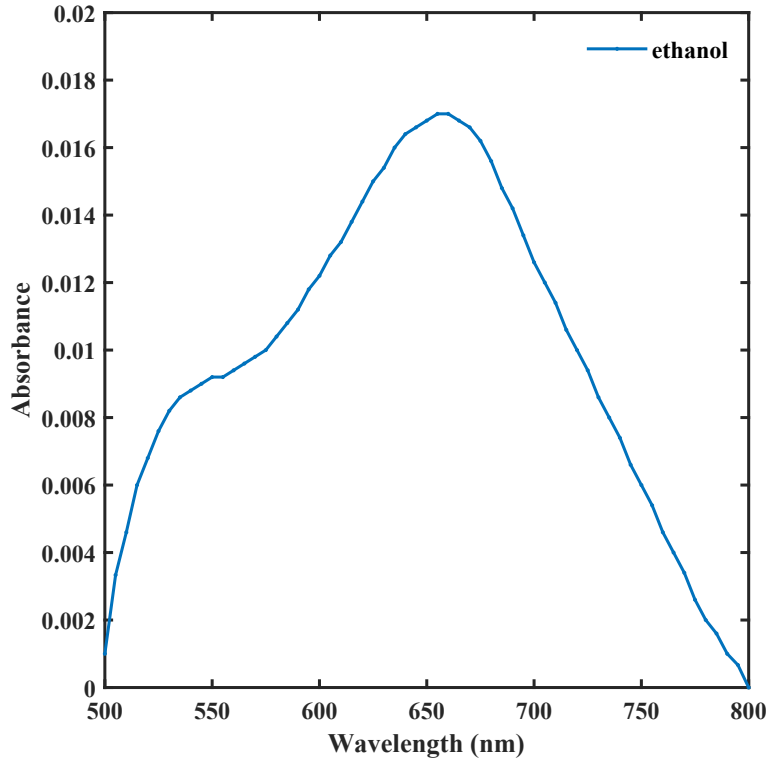

Figure S16 UV-Vis plot used to determine ammonia produced by the indophenol method using ethanol as the proton source.

All the electrochemical studies have been done with the 0.5 mM of Ni_4 compound in THF containing 100 mM of *n*-Bu_4NPF_6 as supporting electrolyte on an electrochemical workstation PGSTAT204-Metrohm multi-Autolab potentiostat/galvanostat using a home-made H-cell (Figure S17) separated by a G4 membrane using a typical three-electrode setup (counter electrode: Pt coil, Ag wire used as a pseudoreference electrode, and glassy carbon as a working electrode (GC) to carry out all the experiments. Before each set of experiments, the reference electrode was calibrated using a ferrocene redox couple. At the end of electrolysis, the electrochemically produced NH_3 in the cathodic chamber was measured by ion chromatographic (IC) analysis.

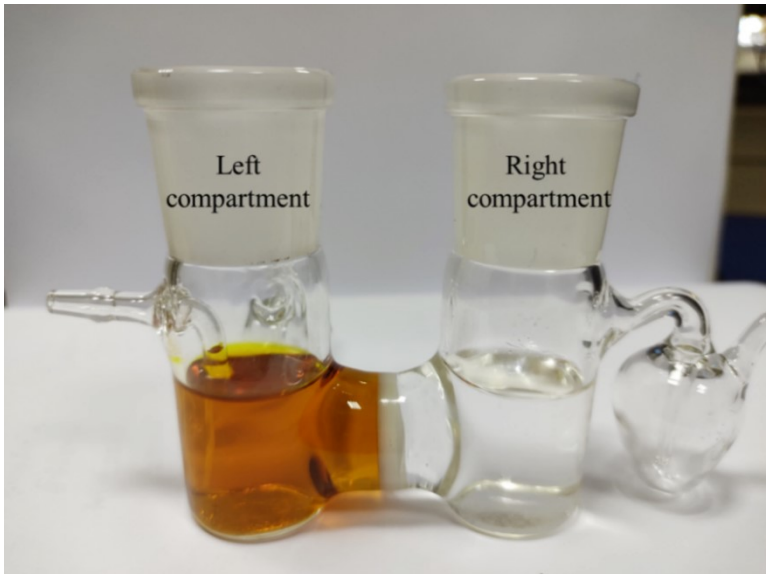

Figure S17 H-cell setup for the controlled potential electrolysis experiment [The working chamber at the left contains 0.5 mM catalyst, 100 mM *n*-Bu_4NPF_6, 100 mM phenol, THF, and the counter chamber at the right contains THF, 100 mM *n*-Bu_4NPF_6.

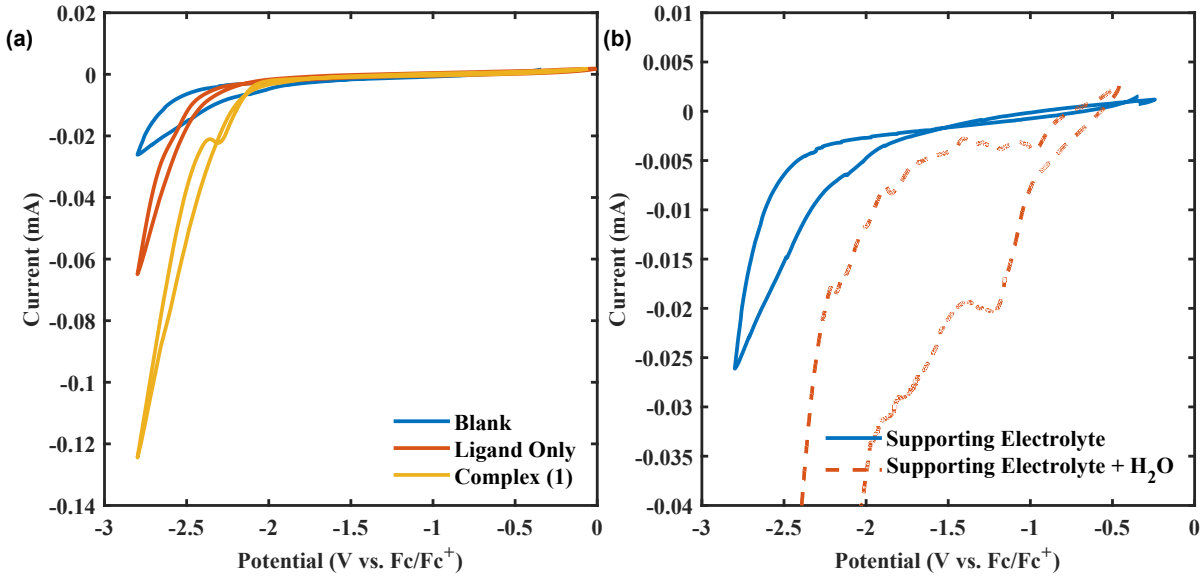

Figure S18 (a) Comparing the CVs of blank alone (0.1 M of *n*-Bu_4NPF_6), 0.5 mM of Schiff base ligand (Me-LH_2) and 0.5 mM of **1** in THF solution under Ar, 0.1 V/s scan rate (glassy carbon (GC) working electrode (3 mm diameter) and Pt counter electrode, 0.1 M *n*-Bu_4PF_6 as a supporting electrolyte). (b) CV of the electrolyte after the external addition of H_2O.

Detection of NH_4^+ by Ion Chromatography (IC):

The concentration of NH_4^+ ion was determined using an IC analysis recorded by the Metrohm Ion Chromatography System (Model no: 930 ECO IC). The flow rate of 1 mL/min was maintained for 3.0 mmol/L nitric acid + 30 % acetone for Figure 7c. For the analysis shown in

Figure 8a, 930 compact IC Flex Oven/ChS/PP (2.930.2300) fitted with IC conductivity detector (2.850.9010) with a flow rate of 1mL/min of 3.0 mmol L^{-1} nitric acid. In both cases, the Metrosep C 3-250/4.0 (6.1010.430) cation exchange column was used to detect possible NH_4^+ and $N_2H_5^+$ ions in a single experiment. Ionic product from the THF solution of the working chamber was extracted using a DCM-H_2O (1:1) mixture. The obtained aqueous layer was filtered using a syringe filter of 0.22 microns, and it was aspirated into the IC instrument fitted with a cationic column. Ammonium chloride (NH_4Cl) is used as a reference standard for NH_4^+ ions to perform quantification. At -2.3 V, the maximum activity of complex **1** has been noticed while comparing the concentration of NH_4^+ produced at different potentials (Figure S19c). All the control experiments were performed using a cathodic solution under identical conditions.

The NH_4^+ was calibrated by recording IC containing various concentrations of NH_4Cl.

The faradaic efficiency (FE) and the NH_3 yield rate (r_{NH_3}) were calculated using equations **1** and (2), respectively.

$$FE\ (\%) = \left(\frac{nFCV}{17 \times Q}\right) \times 100 \qquad (1)$$

$$r_{NH_3} = \frac{C \times V}{t \times A} \qquad (2)$$

Where n is the number of electrons required for the formation of 1 mol of NH_3, F is Faraday constant 96,485 C/mol, C is the concentration of ammonia (in μg/mL), Q is the charge consumed during CPE (C/mole), V is the volume of the electrolyte solution (mL), t is the duration of the electrolysis and A is the area of the electrode (0.07 cm^2).

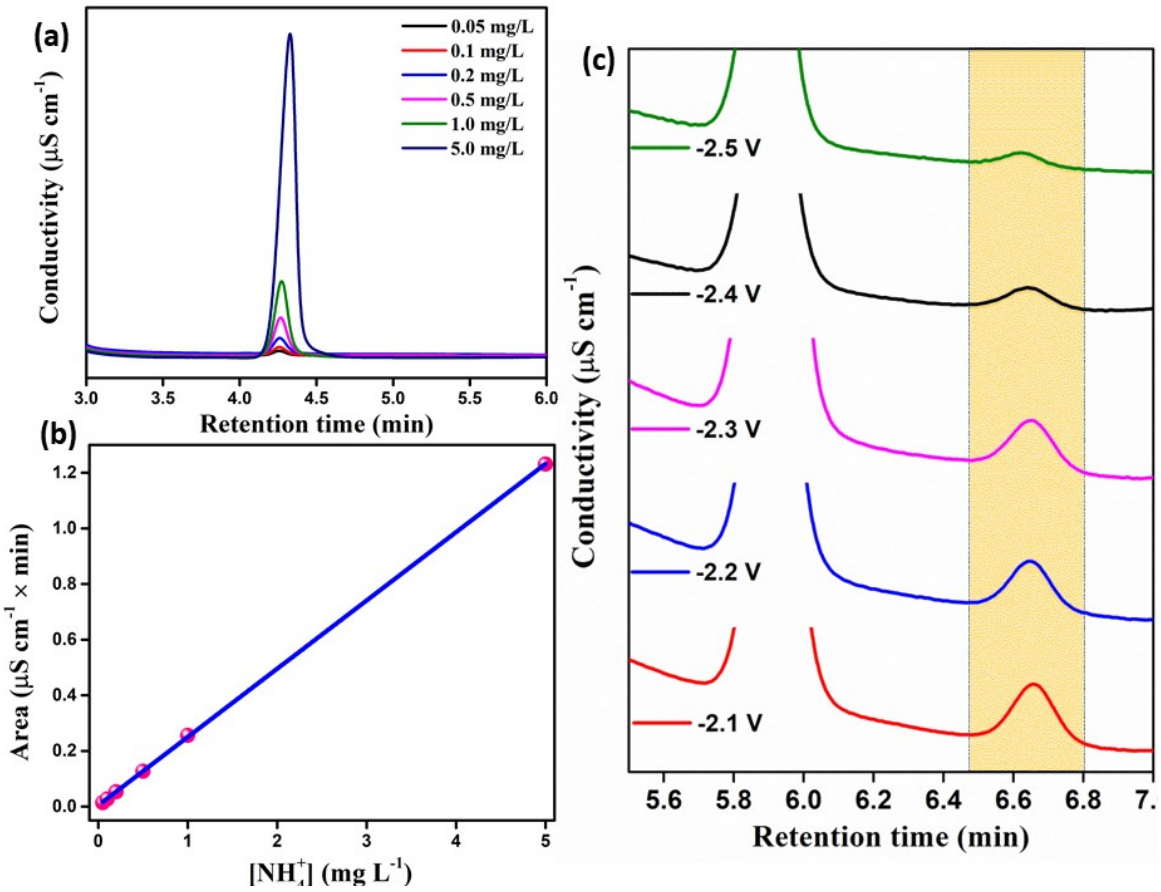

Figure S19 (a) Ion Chromatogram shows the NH_4^+ ion elution time at different concentrations of NH_4Cl. (b) The calibration plot of 0.05-5.0 mg/L of each NH_4Cl standard vs their elution time (c) Ion Chromatogram shows the NH_4^+ ion elution time of post-electrolysis solution at different potentials.

Structural stability post-electrolysis:

EPR measurement:

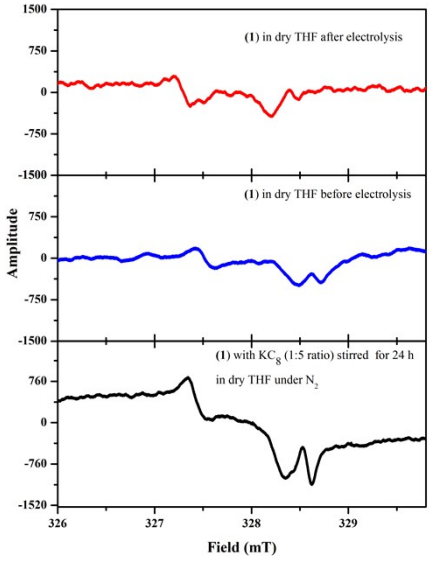

Figure S20 Comparison of X-band EPR spectrum of different sampling solutions at 77K. (microwave power: 1 mW, modulation amplitude: 0.1 mT)

FT-IR and UV-Visible measurements:

Sample preparation:

The solution containing **1** in THF solvent with *n*-Bu_4NPF_6 supporting electrolyte was taken before subjecting it to electrolysis and evaporated to dryness by applying a vacuum. Likewise, following the electrolysis, the post-electrolytic solution underwent vacuum treatment and dried the sample by evaporating the solvent. A comparison of solid-state Fourier-Transform Infrared (FT-IR) spectra of **1** before and after electrochemical NRR showing the retention of the stretching frequencies corresponds to aromatic C-H, C=C, and C=N functional groups, indicating the electrocatalyst was relatively stable even after the electrocatalysis (Figure S21). The intense peaks appearing at 555 cm^{-1} and 842 cm^{-1} can be attributed to the vibrations of Ni-O[S15] and $–NH_{asym}$[S16] in the post-electrolytic sample of **1**.

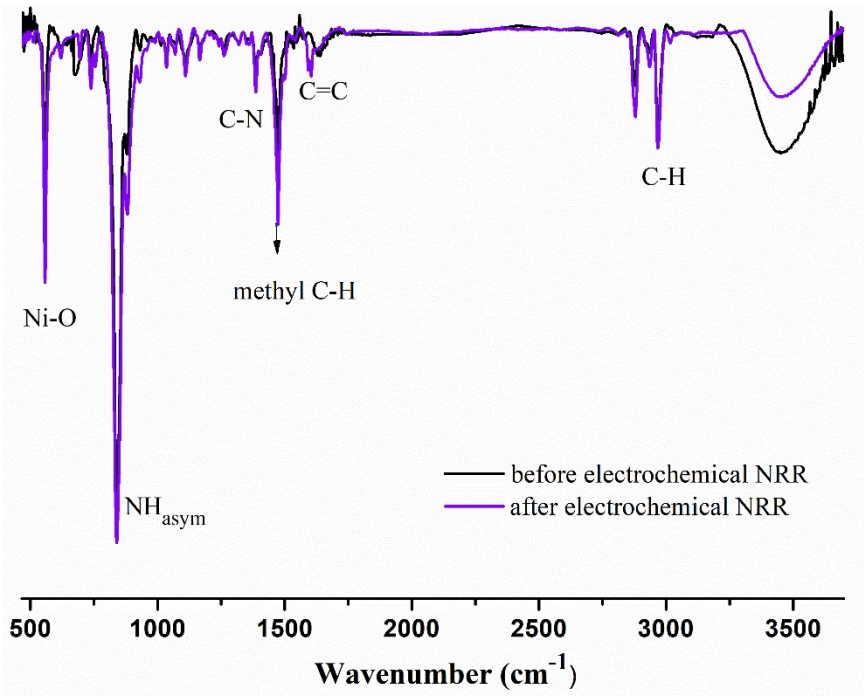

Figure S21 Comparison of solid FT-IR spectra of **1** before and after chronoamperometry.

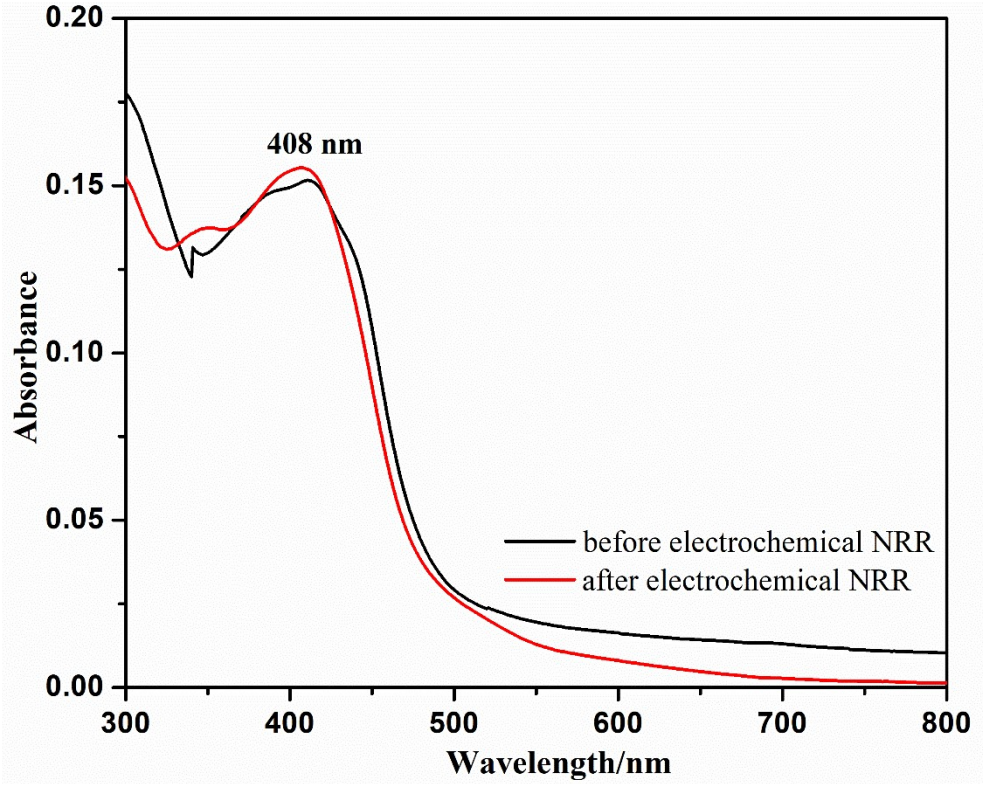

Figure S22 Comparison of solution UV-visible spectra of **1** in THF before and after chronoamperometric experiments.

A comparison of the solution UV-Vis spectra of **1** before and after electrochemical NRR is given in (Figure S22). The peak at 408 nm attributed to the π to π* transition of Ni coordinated Schiff base complex was intact even after electrochemical NRR.[S17]

……

10. DFT and EDA-NOCV calculations:

Computational methods

Geometry optimisations and vibrational frequencies calculations of (L-Me)Ni–N_2 complex (**2**), its reduced state (anionic, dianionic and trianionic) and hydrogen adduct complexes in a singlet, doublet and triplet electronic states have been carried out at the BP86-D3(BJ)/Def2TZVPP in THF using CPCM solvation model.[S18] The absence of imaginary frequencies assures the minima on the potential energy surface. All the calculations were performed using the Gaussian 16 program package.[S19] NBO[S20] calculations have been performed using NBO 6.0 [S21] program to evaluate partial charges, Wiberg bond indices (WBI) [S22] and natural bond orbitals. QTAIM calculations have been performed using the AIMall package.[S23] The nature of the bond in Ni−N complexes was analysed by energy decomposition analysis (EDA)[S24] coupled with natural orbital for chemical valence (NOCV)[S25] using the ADF 2018.105 program

package.[S26] EDA-NOCV calculations were carried out at the BP86-D3(BJ)-ZORA/TZ2P[S27] level using the geometries optimised at BP86-D3(BJ)-ZORA/def2-TZVPP level. The zeroth-order regular approximation (ZORA) included scalar relativistic effects for the metals.[S28] All electrons were considered in the computations. The EDA-NOCV method involves the decomposition of the intrinsic interaction energy (ΔE_{int}) between two fragments into four energy components as follows:

$$\Delta E_{\text{int}} = \Delta E_{\text{elstat}} + \Delta E_{\text{Pauli}} + \Delta E_{\text{orb}} + \Delta E_{\text{disp}} \qquad \mathbf{1}$$

Where the electrostatic ΔE_{elstat} term originated from the quasi-classical electrostatic interaction between the unperturbed charge distributions of the prepared fragments, the Pauli repulsion ΔE_{Pauli} (repulsion energy due to the interactions of same spins between the fragments) is the energy change associated with the transformation from the superposition of the unperturbed electron densities of the isolated fragments to the wave function, which correctly obeys the Pauli principle through explicit anti-symmetrisation and renormalisation of the production of the wavefunction. Dispersion interaction, ΔE_{disp} (equivalent to attractive forces due to instantaneous fluctuation of electron clouds in the fragment before and after the bond formation), is also obtained as we used D3(BJ). The orbital term ΔE_{orb} comes from (constructive interference during spatial mixing of orbitals of the fragments) the mixing of orbitals, charge transfer and polarisation between the isolated components. This can be further divided into contributions from each irreducible representation of the point group of an interacting system as follows:

$$\Delta E_{orb} = \sum_{r} \Delta E_{r} \qquad (2)$$

The combined EDA-NOCV method can partition the total orbital interactions into pairwise contributions of the orbital interactions, which is essential in providing a complete picture of the bonding. The charge deformation $\Delta\rho_k(r)$, which comes from the mixing of the orbital pairs $\psi_k(r)$ and $\psi_{-k}(r)$ of the interacting fragments, gives the magnitude and the shape of the charge flow due to the orbital interactions (Equation 3). The associated orbital energy ΔE_{orb} presents the amount of orbital energy from such interaction (Equation 4).

$$\Delta\rho_{orb}(r) = \sum_{k} \Delta\rho_{k}(r) = \sum_{k=1}^{N/2} \nu_{k}[-\psi_{-k}^{2}(r) + \psi_{k}^{2}(r)] \qquad (3)$$

$$\Delta E_{Orb} = \sum_{k} \Delta E_{Orb}^{k} = \sum_{k} \nu_{k}\left[- F_{-k,-k}^{TS} + F_{k,k}^{TS}\right] \qquad (4)$$

Readers are further referred to the recent review articles to know more about the EDA-NOCV method and its applications. [S29]

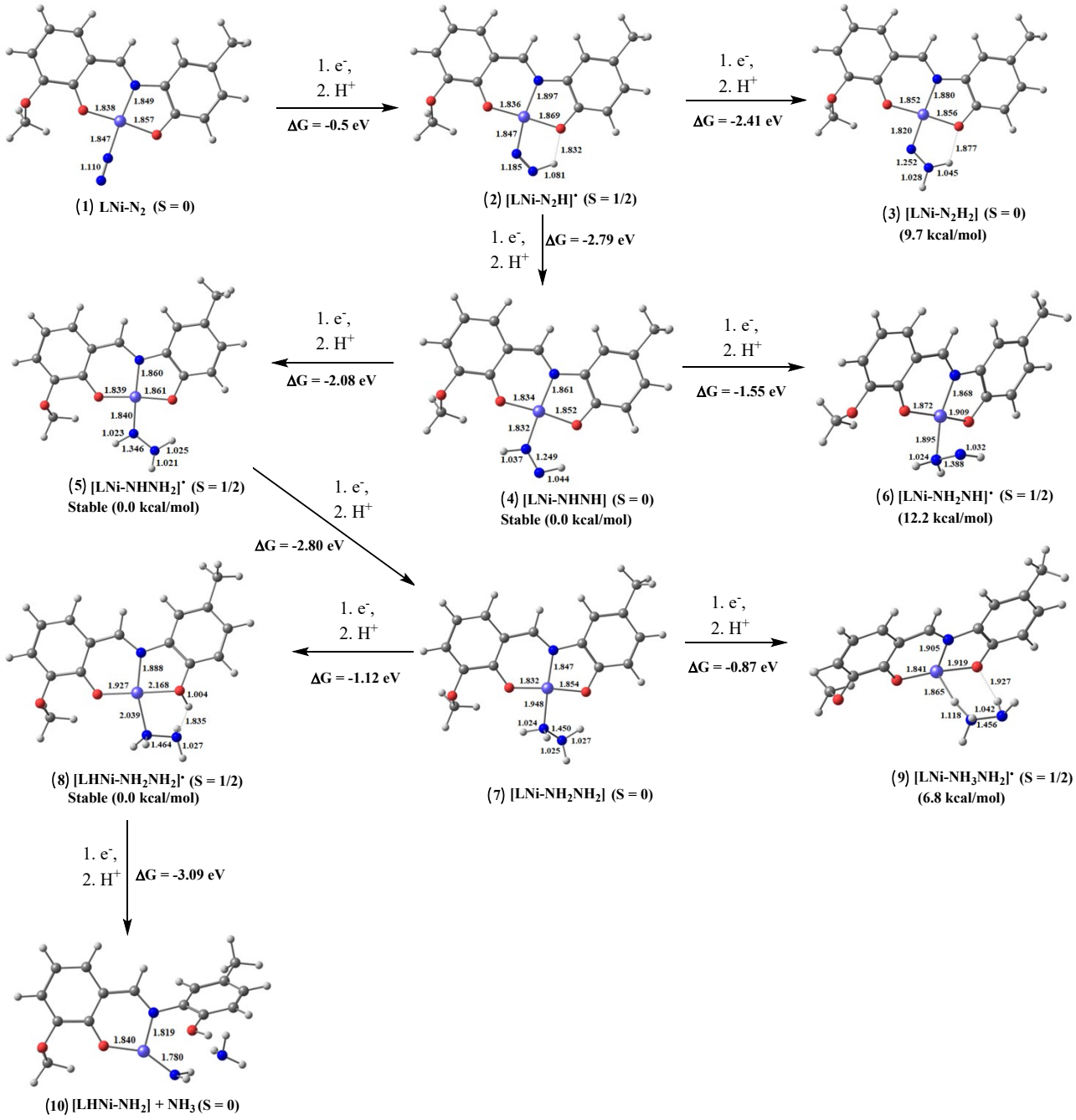

Scheme S2a Schematic representation of overall additions of H-atom (e^- and H^+ addition) to Ni-N_2 with change in Gibbs free energy at BP86-D3(BJ)/Def2TZVPP in THF.

To understand the catalytic mechanism of hydrogen addition to activated N_2, we have optimised a series of (L-Me)Ni-N_2-H complexes depicting the stepwise addition of hydrogen to form NH_3 from N_2. (Scheme S2a) illustrates the preference of H addition to the coordinated and terminal dinitrogen with change in Gibbs free energy and relative energies. Adding first H

to neutral (L)Ni-N_2 on the terminal nitrogen is favourable by 0.5 eV. The addition of second H to (L-Me)Ni-N_2-H is preferred to take place on coordinated N rather than terminal N to form (L-Me)Ni-NH-NH. The further addition of H occurs alternatively on the terminal and coordinated dinitrogen, as shown in (Scheme S2a). The weakening of the Ni-N bond is evident from the lengthening of the Ni–N bond upon stepwise addition of the protons (Scheme S2b). The plot of energy of the intermediates to the energy of activated (L-Me)Ni and N_2 is shown in (Scheme S2c). (Scheme S2b) shows the energetics of the alternating path for releasing first ammonia from LNi-N_2 molecule in terms of change in Gibbs free energies.

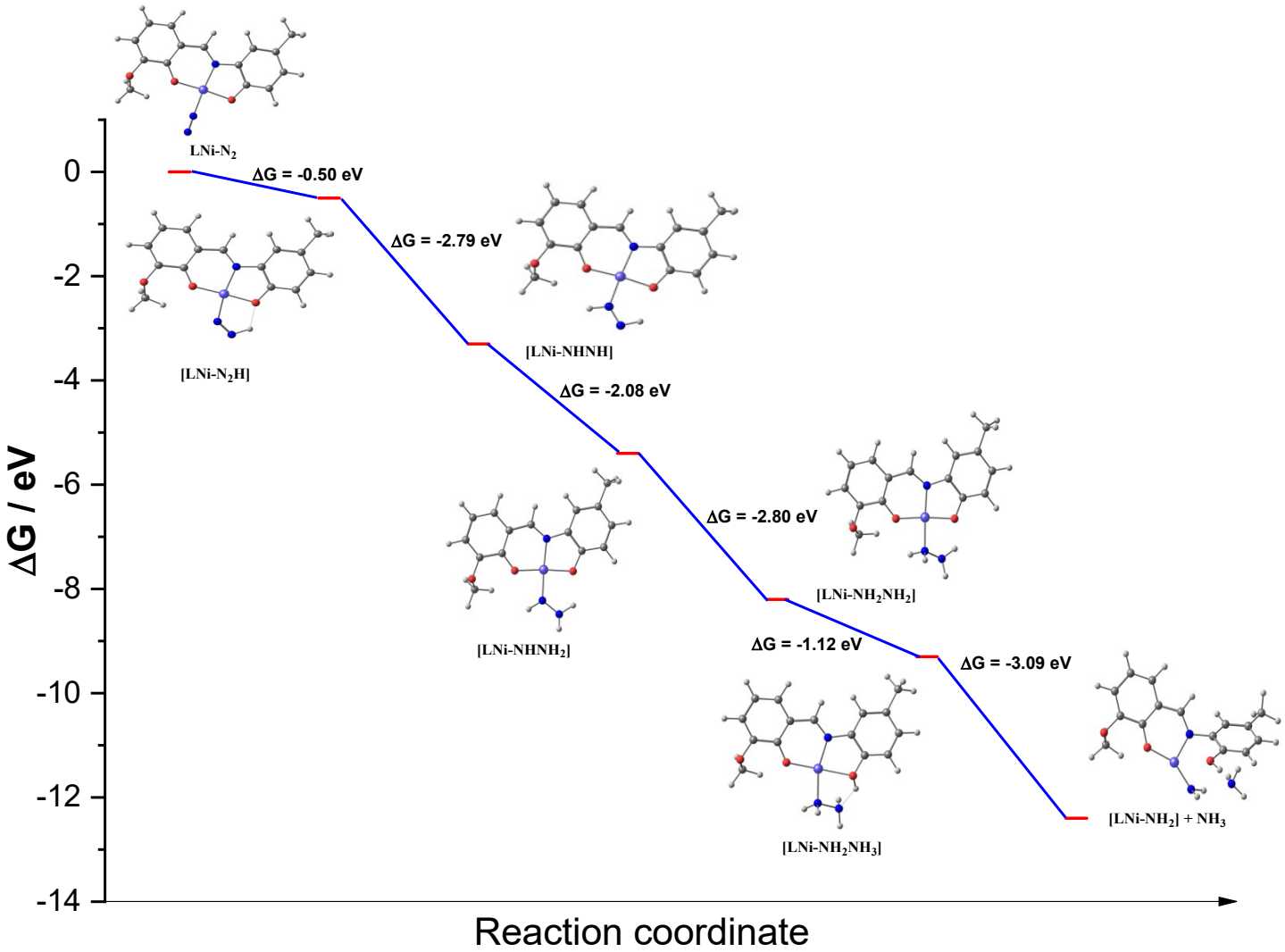

Scheme S2b Plot of change in Gibbs free energy of the intermediates in 'alternating' pathway at BP86-D3(BJ)/Def2TZVPP in THF.

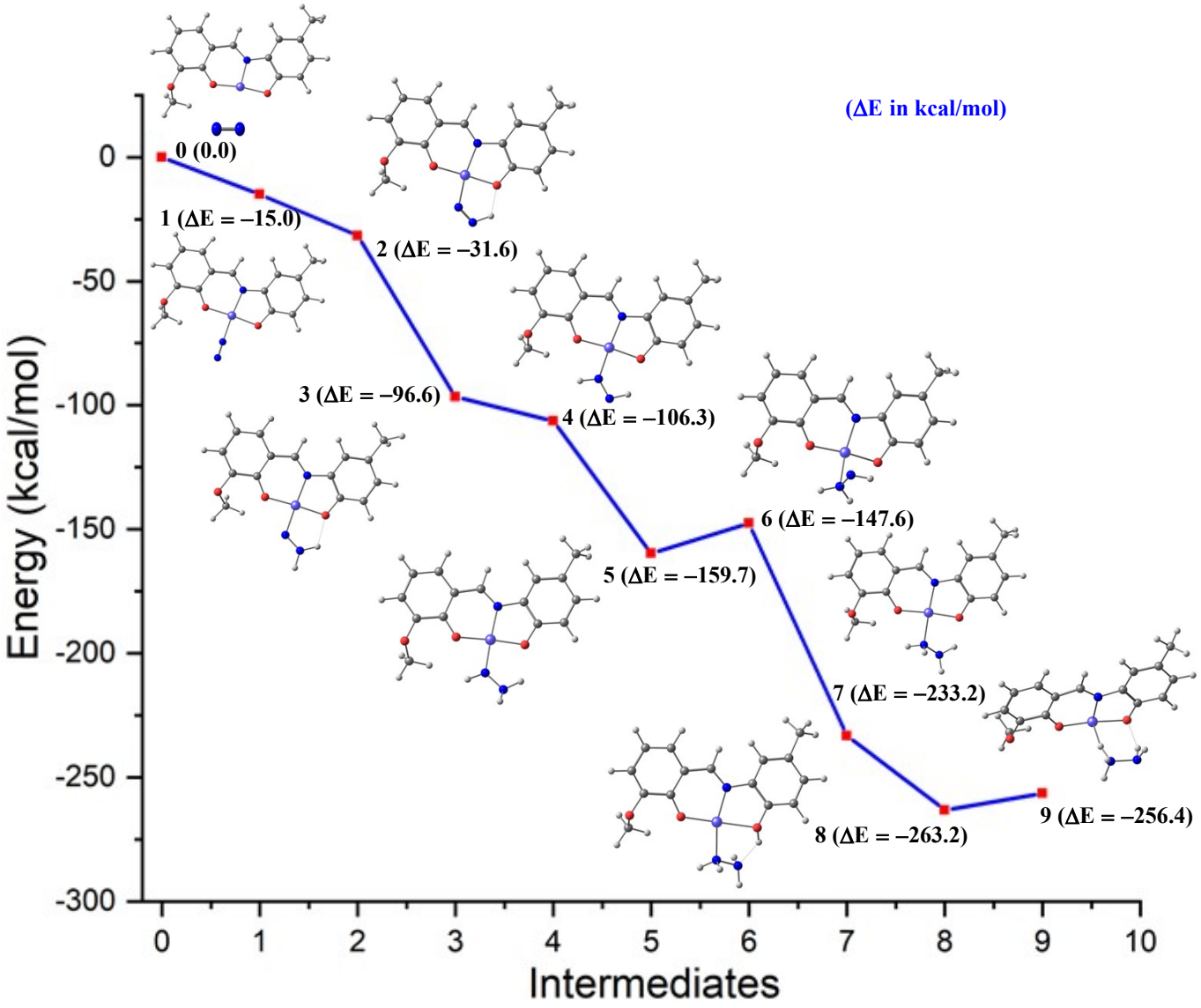

Scheme S2c Plot of energy of the intermediates to the energy of activated (L-Me)Ni and N_2 at BP86-D3(BJ)/Def2TZVPP in THF. and N_2 at BP86-D3(BJ)/Def2TZVPP in THF.

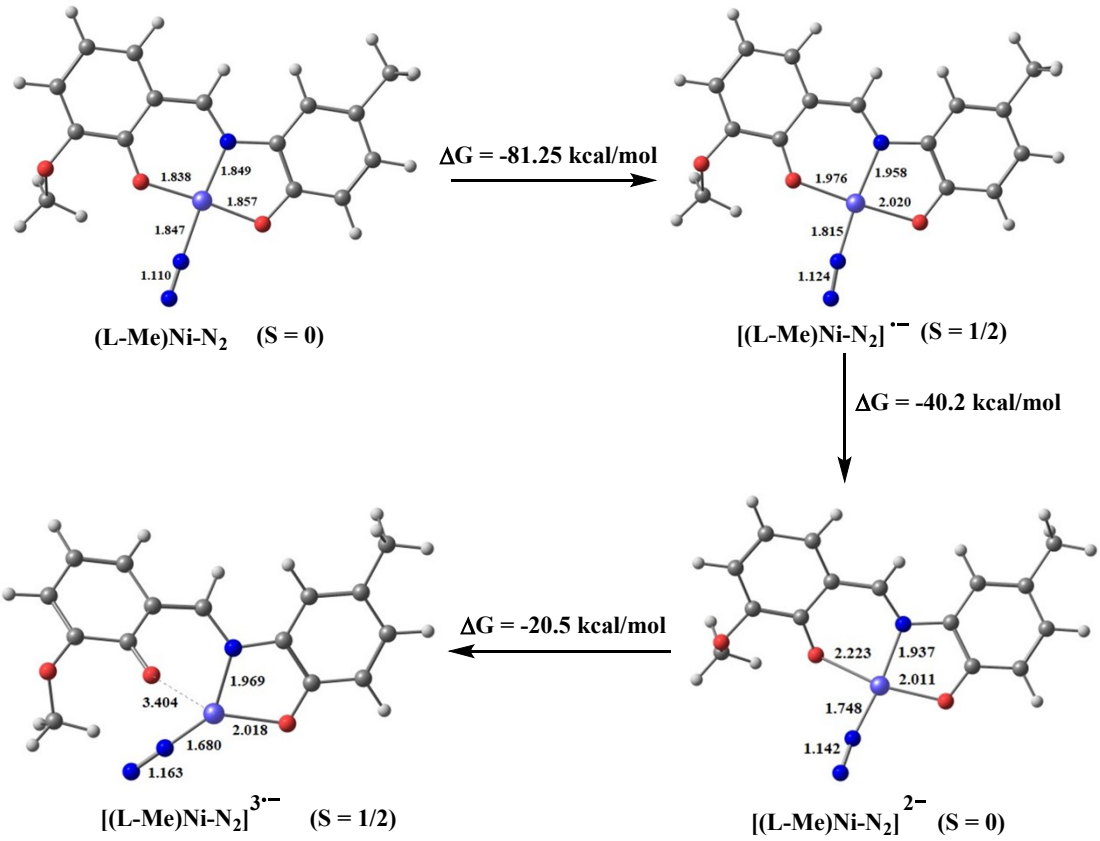

Scheme S3 Gibbs free energy change in the reduction of (L-Me)Ni-N_2 (**2**) in THF.

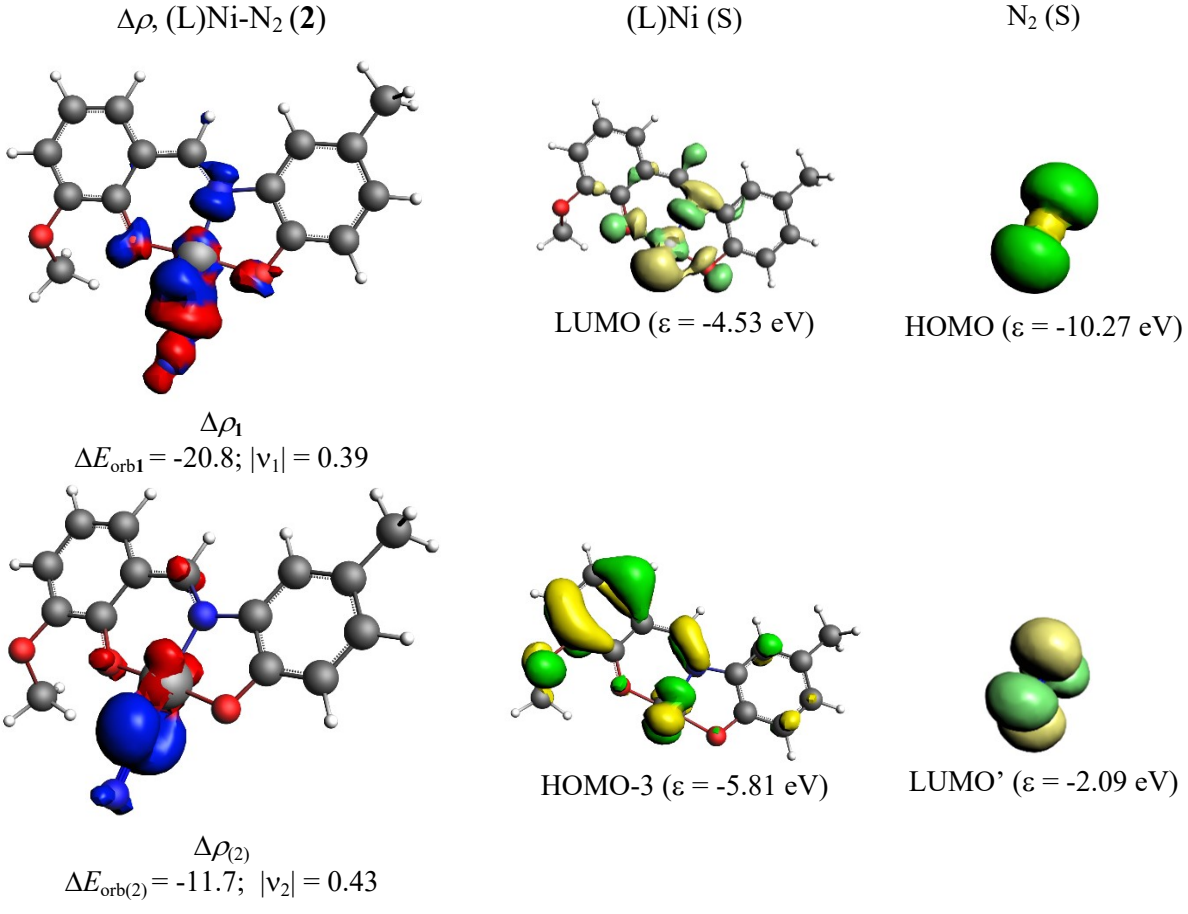

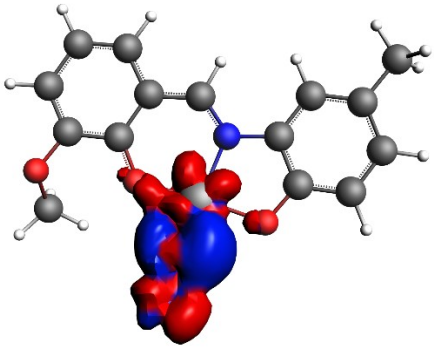

$\Delta\rho_{(3)}$
$\Delta E_{orb(3)}$ = -7.9; $|\nu_3|$ = 0.28

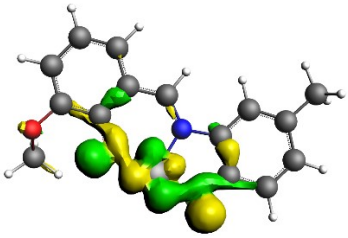

HOMO-5 (ε = -6.36 eV)

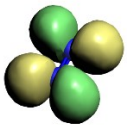

LUMO (ε = -2.09 eV)

Figure S23 The shape of the deformation densities $\Delta\rho_{\mathbf{1}\text{-}(3)}$ that correspond to $\Delta E_{orb\mathbf{1}\text{-}(3)}$, and the associated MOs of (L-Me)Ni-N_2 (**2**) and the fragments orbitals of (L-Me)Ni in singlet state and N_2 in the singlet state at the BP86-D3(BJ)/TZ2P level. Isosurface values of 0.001 au for $\Delta\rho_{(1\text{-}3)}$. The eigenvalues $|\nu_n|$ give the size of the charge migration in e. The direction of the charge flow of the deformation densities is red→blue.

$\Delta\rho$, [(L-Me)NiN_2]$^-$ (**2**) | [(L-Me)Ni]$^-$ (D) | N_2 (S)

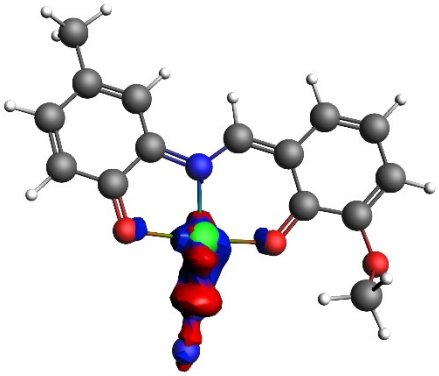

$\Delta\rho_{\mathbf{1}}$
$\Delta E_{orb\mathbf{1}}$ = -28.0; $|\nu_1|$ = 0.54

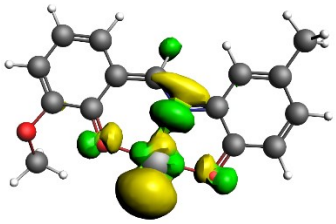

SOMO (ε = 0.18 eV)

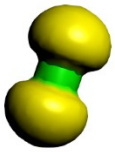

HOMO (ε = -10.26 eV)

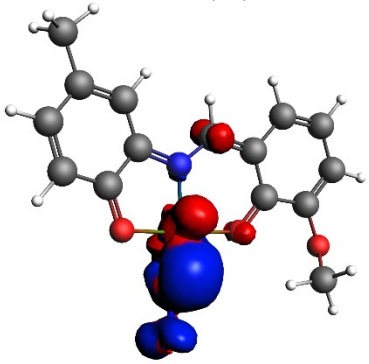

$\Delta\rho_{(2)}$
$\Delta E_{orb(2)}$ = -21.0; $|\nu_2|$ = 0.57

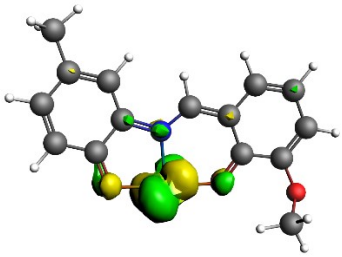

HOMO-2 (ε = -0.82 eV)

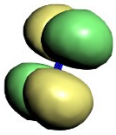

LUMO' (ε = -2.26 eV)

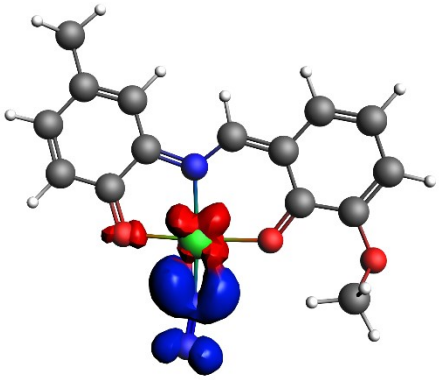

$\Delta\rho_{(3)}$
$\Delta E_{orb(3)}$ = -16.5; $|\nu_3|$ = 0.46

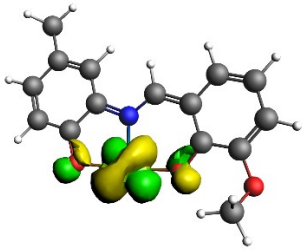

HOMO-3 (ε = -0.94 eV)

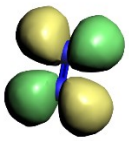

LUMO (ε = -2.26 eV)

Figure S24 The shape of the deformation densities $\Delta\rho_{\mathbf{1}\text{-}(3)}$ that correspond to $\Delta E_{orb\mathbf{1}\text{-}(3)}$, and the associated MOs of [(L-Me)Ni-N_2]$^-$ (**2**$^-$) and the fragments orbitals of [(L-Me)Ni]$^-$ in doublet state and N_2 in the singlet state at the BP86-D3(BJ)/TZ2P level. Isosurface values of 0.001 au for $\Delta\rho_{(1\text{-}3)}$. The eigenvalues $|\nu_n|$ give the size of the charge migration in e. The direction of the charge flow of the deformation densities is red→blue.

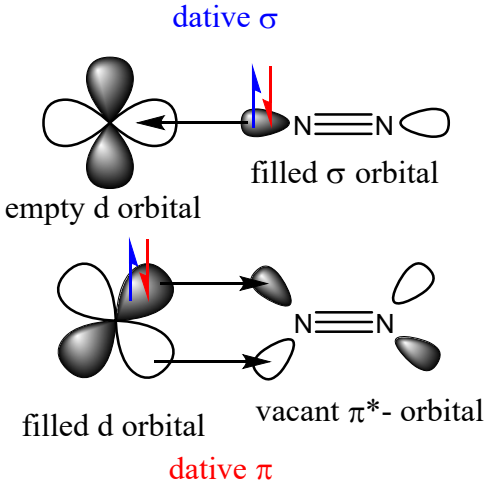

Scheme S4 Bonding model for EDA-NOCV calculation of Ni–N_2 bond of (L-Me)Ni–N_2

11. References

[S1] S. K. Kushvaha, M. Francis, J. Kumar, E. Nag, P. Ravichandran, S. Roy, K. C. Mondal, *RSC Adv*., 2021, **11**, 22849-22858.

[S2] Similar EPR spectrum of Ni(I) complex was reported by: S. Pfirrmann, C. Limberg, C. Herwig, R. Stößer, B. A. Ziemer, *Angew. Chem. Int. Ed*. 2009, **48**, 3357.

[S3] Bruker (2008). APEX2 (Version 2008.1-0). Bruker AXS Inc., Madison, Wisconsin, USA.

[S4] Bruker (2001b). SAINT-V6.28A. Data Reduction Software.

[S5] G. M. Sheldrick, (1996). SADABS. Program for Empirical Absorption Correction. University of Gottingen, Germany.

[S6] L. J. Farrugia, *J. Appl. Cryst*., 1999, **32**, 837.

[S7] G. M. Sheldrick, (1997) SHELXL-97. Program for the Refinement of Crystal.

[S8] G.M. Sheldrick, Acta Cryst., 1990, *A46*, 467.

[S9] A. Majumdar, S.C. Das, T. Shripathi, and R. Hippler. *Compos. Interfaces*, 2012, **19**, 161-170.

[S10] W. Min, D. Xu, P. Chen, G. Chen, Q. Yu, H. Qiu, and X. Zhu. *J. Mater. Sci. Mater. Electron*., 2021, **32**, 8000-8016.

[S11] J. Shi, X. Li, T. Yang, X. Tian, Y. Liu, S. Lei, Y. Song, and Z. Liu. *J. Mater. Sci*., 2021, **56**, 7520-7532.

[S12] Y. Koshtyal, D. Nazarov, I. Ezhov, I. Mitrofanov, A. Kim, A. Rymyantsev, O. Lyutakov, A. Popovich, and M. Maximov, *Coat*., 2019, **9**, 301.

[S13] D. Ghosh, R. Banerjee, G. R. Bhadu, S. N. Bhaduri, A. Mondal, D. N. Srivastava, and P. Biswas, *Mater. Adv*., 2022, **3**, 6831-6841.

[S14] F. Sun, S. Wang, Y. Wang, J. Zhang, X. Yu, Y. Zhou, and J. Zhang, *Sens*., 2019, **19**, 2938.

[S15] B. S. Rathore, N. P. S. Chauhan, S. Jadoun, S. C. Ameta, and R. Ameta, *J. Mol. Struct*., 2021, **1242**, 130750.

[S16] J. M. Ramos, M. T. D. M. Cruz, A. C. Costa Jr, O. Versiane, and C. A. T. Soto, *Sci. Asia*., 2011, **37**, 247-255.

[S17] S. Thakurta, M. Maiti, R. J. Butcher, C. J. Gómez-García, and A. A Tsaturyan, *Dalton Trans*. 2021, **50**, 2200-2209.

[S18] a) A. D. Becke, *Phys. Rev. A.* 1988, **38**, 3098-3100; b) J. P. Perdew, *Phys. Rev. B.* 1986, **33**, 8822-8824; c) S. Grimme, S. Ehrlich, L. Goerigk, *J. Comput. Chem.* 2011, **32***,* 1456-1465; d) S. Grimme, J. Antony, S. Ehrlich, H. *J.* Krieg, *Chem. Phys.* 2010, **132***,* 154104 (1-19); e) F. Weigend, R. Ahlrichs, *Phys. Chem. Chem. Phys.* 2005, **7**, 3297-3305; f) F. Weigend, *Phys. Chem. Chem. Phys.* 2006, **8***,* 1057; g) M. Cossi, N. Rega, G. Scalmani, V. Barone, *J. Comput. Chem.* 2003, **24**, 669-681.

[S19] a) M. J. Frisch, *et al*, *Gaussian 16, Revision A.03*, Gaussian, Inc., Wallingford CT. 2016.

[S20] a) F. Weinhold, C. Landis, *Valency and Bonding, A Natural Bond Orbital Donor – Acceptor Perspective,* Cambridge University Press, Cambridge, 2005; b) C. R. Landis, F. Weinhold, *The Chemical Bond: Fundamental Aspects of Chemical Bonding,* Wiley, 2014, 91-120; c) F. M. Bickelhaupt, E. J. Baerends, *Rev. Comput. Chem*. 2000, **15**, 1−86.

[S21] K. B. Wiberg, *Tetrahedron* 1968, **24**, 1083-1096.

[S22] E. D. Glendening, C. R. Landis, F. Weinhold, *J. Comput. Chem*. 2013, **34**, 1429-1437.

[S23] a) R. F. W. Bader, *Oxford University Press*, Oxford, 1990; b) T. A. Keith, *AIMAll* (Version 15.05.18), TK Gristmill Software, Overland Park KS, USA, 2015 (aim.tkgristmill.com).

[S24] T. Ziegler, A. Rauk, *Theor. Chim. Acta.* 1977, **46**, 1-10.

[S25] a) M. Mitoraj, A. Michalak, *Organometallics* 2007, **26**, 6576-6580; b) M. Mitoraj, A. Michalak, *J. Mol. Model.* 2008, **14**, 681-687; c) M. Mitoraj, A. Michalak, T. Ziegler, *Phys. Chem. A.* 2008, **112**, 1933-1939; d) M. Mitoraj, A. Michalak, T. Ziegler, *J. Chem. Theory Comput.* 2009, **5**, 962-975.

[S26] a) *ADF2017*, SCM, Theoretical Chemistry, Vrije Universiteit, Amsterdam, The Netherlands, http://www.scm.com; b) G. te Velde, F. M. Bickelhaupt, E. J. Baerends, C. F. Guerra, S. J. A. van Gisbergen, J. G. Snijders, T. Ziegler, *J. Comput. Chem.* 2001, **22**, 931-967.

[S27] a) E. van Lenthe, E. J. Baerends, *J. Comput. Chem*. 2003, **24**, 1142-1156; b) E. van Lenthe, E. J. Baerends, J. G. Snijders, *J. Chem. Phys*. 1994, **101**, 9783-9792

[S28] a) Ch. Chang, M. Pelissier, Ph. Durand, *Phys. Scr*. 1986, **34**, 394-404; J.-L. Heully, I. Lindgren, E. Lindroth, S. Lundqvist, A.-M. Martensson-Pendrill, *J. Phys. B.* 1986, **19**, 2799-2815; c) E. van Lenthe, E. J. Baerends, J. G. Snijders, *J. Chem. Phys*. 1993, **99**, 4597-4610.

[S29] a) G. Frenking, F.M. Bickelhaupt, *The Chemical Bond: Fundamental Aspects of Chemical Bonding*, *The EDA Perspective of Chemical Bonding,* Wiley-VCH: Weinheim, 2014; b) L. Zhao, M. v. Hopffgarten, D. M. Andrada, G. Frenking, *WIREs Comput. Mol. Sci.* 2017, **8**, e1345; c) L. Zhao, M. Hermann, W. H. E. Schwarz, G. Frenking, *Nat. Rev. Chem.* 2019, **3**, 48-63; d) W. Yang, K. E. Krantz, L. A. Freeman, D. Dickie, A. Molino, G. Frenking, S. Pan, D. J. D. Wilson, R. J. Gilliard Jr., *Angew. Chem. Int. Ed.*, 2020, **59**, 3850-3854; e) G. Deng, S. Pan, G. Wang, L. Zhao, M. Zhou, G. Frenking, *Angew. Chem. Int. Ed*., 2020, **59**, 10603-10609; f) S. Pan, G. Frenking, *Angew. Chem. Int. Ed*., 2020, **59**, 8756-8759; g) L. Zhao, S. Pan, M. Zhou, G. Frenking, *Science*, 2019, **365**, 1-4; h) R. Saha, S. Pan, P. K. Chattaraj, G. Merino, *Dalton Trans*., 2020, **49**, 1056-1064.

12. Optimised Coordinates

Electronic Energies in Hartree

L-Ni–N_2 Singlet
Energy: -2478.5139291

6	-4.101409000	-2.080478000	-0.139543000
6	-3.600412000	-0.787109000	-0.112746000
6	-2.185324000	-0.558272000	-0.101703000
6	-1.325072000	-1.702735000	-0.075288000
6	-1.878808000	-3.012589000	-0.099602000
6	-3.244945000	-3.201357000	-0.141460000
1	-5.184941000	-2.205409000	-0.160690000
1	-1.198356000	-3.865448000	-0.087548000
1	-3.666166000	-4.205947000	-0.163642000

8	-4.485340000	0.264571000	-0.181767000
8	-1.758594000	0.680909000	-0.135537000
6	0.087204000	-1.561263000	-0.042119000
1	0.669652000	-2.487048000	-0.024860000
7	0.754491000	-0.428641000	-0.028765000
6	2.169224000	-0.356741000	0.017387000
6	2.622419000	0.976833000	-0.004476000
6	3.070576000	-1.430668000	0.080685000
6	4.007716000	1.227867000	0.033972000
6	4.445149000	-1.185483000	0.118625000
1	2.716412000	-2.461895000	0.103318000
6	4.891940000	0.154935000	0.093710000
1	4.365266000	2.257787000	0.016323000
1	5.965355000	0.354588000	0.123204000
6	-4.468227000	1.160731000	0.949613000
1	-3.489721000	1.647391000	1.055745000
1	-5.240394000	1.911938000	0.750504000
1	-4.715842000	0.611834000	1.871861000
8	1.708382000	1.948244000	-0.061566000
28	-0.012419000	1.252118000	-0.097539000
6	5.436485000	-2.320969000	0.185950000
1	4.928205000	-3.293957000	0.196160000
1	6.120549000	-2.306567000	-0.676239000
1	6.059360000	-2.255833000	1.091114000
7	-0.646330000	2.985899000	-0.170665000
7	-1.001922000	4.036062000	-0.216461000

L-Ni–N_2 Triplet
Energy: -2478.4871864

6	-4.112218000	-2.146083000	-0.145063000
6	-3.626808000	-0.839698000	-0.090519000
6	-2.217950000	-0.574925000	-0.090706000
6	-1.336676000	-1.713585000	-0.081656000
6	-1.871249000	-3.023318000	-0.125890000
6	-3.240591000	-3.243989000	-0.170641000
1	-5.193863000	-2.286935000	-0.164204000
1	-1.177334000	-3.866141000	-0.129562000
1	-3.638217000	-4.257589000	-0.210718000
8	-4.549758000	0.176338000	-0.124670000
8	-1.814936000	0.672904000	-0.121720000
6	0.094094000	-1.599053000	-0.051527000
1	0.642683000	-2.550873000	-0.042734000
7	0.759905000	-0.477067000	-0.033128000
6	2.168340000	-0.399356000	0.013783000
6	2.644921000	0.946321000	-0.013203000
6	3.065852000	-1.465734000	0.093229000
6	4.036080000	1.168919000	0.037540000
6	4.451522000	-1.238774000	0.139959000
1	2.701914000	-2.494304000	0.125204000
6	4.915225000	0.090747000	0.112888000
1	4.402278000	2.196136000	0.022103000
1	5.989958000	0.278612000	0.156315000
6	-4.482888000	1.148729000	0.941919000
1	-3.545617000	1.716213000	0.904517000
1	-5.339206000	1.814636000	0.788493000
1	-4.579099000	0.644987000	1.916498000
8	1.770167000	1.943530000	-0.077954000
28	-0.031150000	1.331412000	-0.108020000
6	5.417399000	-2.393578000	0.191105000
1	4.964034000	-3.276662000	0.661132000
1	5.734457000	-2.688766000	-0.822489000
1	6.325501000	-2.130476000	0.750430000
7	-0.676292000	3.186319000	-0.182183000
7	-0.810668000	4.287849000	-0.199400000

L-Ni–N_2 Radical Anion
Energy: -2478.6378907

6	-4.103111000	-2.177538000	-0.081229000
6	-3.647720000	-0.868884000	-0.113709000
6	-2.241156000	-0.554374000	-0.135379000

6	-1.328012000	-1.672611000	-0.054135000	6	-4.113274000	-1.998894000	-0.511829000
6	-1.839722000	-2.999646000	-0.010522000	6	-3.626383000	-0.798322000	-0.000001000
6	-3.196982000	-3.259445000	-0.037753000	6	-2.225205000	-0.530319000	0.164956000
1	-5.181412000	-2.348438000	-0.091716000	6	-1.310726000	-1.563355000	-0.315344000
1	-1.122804000	-3.823179000	0.040699000	6	-1.848079000	-2.761417000	-0.870822000
1	-3.569284000	-4.284006000	-0.013415000	6	-3.212798000	-2.988334000	-0.966929000
8	-4.587702000	0.144105000	-0.214098000	1	-5.194040000	-2.153733000	-0.550809000
8	-1.870472000	0.686363000	-0.231334000	1	-1.143673000	-3.516254000	-1.235767000
6	0.092069000	-1.520843000	-0.003742000	1	-3.591434000	-3.925654000	-1.380093000
1	0.650923000	-2.458687000	0.127076000	8	-4.562408000	0.175219000	0.360930000
7	0.763191000	-0.390773000	-0.068484000	8	-1.804192000	0.586481000	0.675136000
6	2.166649000	-0.349320000	0.011822000	6	0.095214000	-1.358860000	-0.359911000
6	2.688646000	0.979465000	0.146745000	1	0.674828000	-2.106437000	-0.928564000
6	3.033207000	-1.455611000	-0.043263000	7	0.767275000	-0.288546000	0.108349000
6	4.099529000	1.115007000	0.238034000	6	2.161396000	-0.317033000	0.097296000
6	4.419488000	-1.304136000	0.044236000	6	2.770269000	0.962442000	-0.147583000
1	2.627097000	-2.461598000	-0.173088000	6	2.961367000	-1.452783000	0.308889000
6	4.933857000	0.002811000	0.191804000	6	4.175494000	1.046048000	-0.066844000
1	4.513715000	2.119844000	0.344646000	6	4.367040000	-1.359809000	0.356578000
1	6.016133000	0.143180000	0.262921000	1	2.478637000	-2.419964000	0.475240000
6	-4.577110000	1.083467000	0.877681000	6	4.956432000	-0.101424000	0.166271000
1	-3.602518000	1.583653000	0.955468000	1	4.651123000	2.015713000	-0.237594000
1	-5.361462000	1.817740000	0.657498000	1	6.046871000	-0.012961000	0.194367000
1	-4.812743000	0.569583000	1.824840000	6	-4.573123000	0.475112000	1.764332000
8	1.872614000	2.005243000	0.185681000	1	-3.581100000	0.811947000	2.095983000
28	-0.030809000	1.398278000	-0.112490000	1	-5.312344000	1.274262000	1.910462000
6	5.344964000	-2.494726000	-0.035619000	1	-4.879798000	-0.413023000	2.346715000
1	4.778462000	-3.434977000	-0.084165000	8	1.982518000	1.973763000	-0.469762000
1	5.992016000	-2.450249000	-0.926697000	28	0.059501000	1.499265000	-0.121640000
1	6.011666000	-2.550847000	0.839441000	6	5.207464000	-2.584024000	0.638754000
7	-0.587208000	3.116050000	-0.292734000	1	4.940843000	-3.426054000	-0.020440000
7	-0.813161000	4.217409000	-0.282440000	1	6.276511000	-2.371317000	0.491827000
				1	5.083673000	-2.942780000	1.674998000
				7	-0.753791000	3.024577000	-0.381672000

L-Ni–N_2 Di-anion
Energy: -2478.7012793

7	-1.121200000	4.022392000	-0.799208000

L-Ni–N_2 Tri-anion
Energy: -2478.7390586

6	-4.108793000	-2.006060000	0.499694000
6	-3.608970000	-1.067444000	-0.410885000
6	-2.205037000	-0.827542000	-0.636328000
6	-1.299324000	-1.461344000	0.347943000
6	-1.847819000	-2.454806000	1.218228000
6	-3.209805000	-2.740770000	1.296971000
1	-5.190549000	-2.152136000	0.566342000
1	-1.151294000	-2.981557000	1.881571000
1	-3.577507000	-3.499016000	1.993243000
8	-4.556396000	-0.425116000	-1.227451000
8	-1.798609000	-0.134857000	-1.642653000
6	0.105250000	-1.225782000	0.437999000
1	0.669501000	-1.997774000	0.994023000
7	0.808079000	-0.107389000	0.093081000
6	2.181754000	-0.211939000	-0.042009000
6	2.883284000	1.057560000	-0.086807000
6	2.925630000	-1.410340000	-0.147526000
6	4.283407000	1.035067000	-0.243007000
6	4.331074000	-1.410493000	-0.285387000
1	2.390735000	-2.364686000	-0.160638000
6	4.999130000	-0.180981000	-0.334094000
1	4.812977000	1.992759000	-0.275165000
1	6.088503000	-0.162314000	-0.445034000
6	-4.452505000	1.004623000	-1.176088000
1	-3.441137000	1.321020000	-1.473853000
1	-5.202484000	1.404040000	-1.874112000
1	-4.669637000	1.373405000	-0.156830000
8	2.180140000	2.168303000	0.031680000
28	0.227186000	1.758557000	0.331994000
6	5.089189000	-2.715533000	-0.378570000
1	5.040780000	-3.295580000	0.560163000
1	4.688291000	-3.370483000	-1.170575000
1	6.152740000	-2.539774000	-0.600408000
7	-1.092696000	2.713130000	0.741912000
7	-1.997098000	3.374339000	1.052440000

L-Ni–N_2 –H Neutral
Energy: -2479.0512385

6	-4.245300000	-1.942200000	-0.068778000
6	-3.691645000	-0.673372000	-0.161568000
6	-2.268632000	-0.493958000	-0.147000000
6	-1.453317000	-1.666371000	0.013167000
6	-2.063531000	-2.946715000	0.114712000
6	-3.435475000	-3.088694000	0.062751000
1	-5.332572000	-2.026061000	-0.100263000
1	-1.418534000	-3.819755000	0.227879000
1	-3.895350000	-4.073877000	0.134647000
8	-4.536812000	0.395999000	-0.354230000
8	-1.798002000	0.721157000	-0.293536000
6	-0.031413000	-1.598135000	0.063958000
1	0.493962000	-2.547915000	0.214310000
7	0.681528000	-0.501703000	-0.044356000
6	2.093433000	-0.472156000	-0.020328000
6	2.606206000	0.843531000	-0.098853000
6	2.962467000	-1.570397000	0.053113000
6	3.995851000	1.046744000	-0.054140000
6	4.346551000	-1.374483000	0.089823000
1	2.570722000	-2.587872000	0.086070000
6	4.843291000	-0.053774000	0.038962000
1	4.389331000	2.062373000	-0.105011000
1	5.922759000	0.108011000	0.068026000
6	-4.483789000	1.422292000	0.659680000
1	-3.496671000	1.902230000	0.687132000
1	-5.250512000	2.155109000	0.384773000
1	-4.720789000	0.993312000	1.646271000
8	1.725011000	1.843020000	-0.251956000

28	-0.044090000	1.247229000	-0.161753000
6	5.293909000	-2.543389000	0.191312000
1	4.754823000	-3.498877000	0.157468000
1	6.025186000	-2.536050000	-0.630834000
1	5.866989000	-2.512196000	1.130725000
7	-0.442441000	3.028481000	0.120105000
7	0.336810000	3.887565000	0.364524000
1	1.360698000	3.543794000	0.322874000

L-Ni–N_2–H Proton
Energy: -2478.850742

6	-4.061796000	-2.192005000	0.001808000
6	-3.598503000	-0.891489000	-0.147414000
6	-2.169216000	-0.647762000	-0.190569000
6	-1.279866000	-1.772158000	0.065092000
6	-1.814590000	-3.071340000	0.240093000
6	-3.180636000	-3.274872000	0.192004000
1	-5.140148000	-2.351752000	-0.010339000
1	-1.132536000	-3.902022000	0.421609000
1	-3.590528000	-4.274476000	0.331708000
8	-4.524814000	0.070668000	-0.361376000
8	-1.747436000	0.528631000	-0.510605000
6	0.120280000	-1.608600000	0.133852000
1	0.706081000	-2.520917000	0.281183000
7	0.770221000	-0.457461000	0.045642000
6	2.157274000	-0.379967000	-0.019499000
6	2.613115000	0.980248000	-0.114672000
6	3.078911000	-1.439827000	0.000245000
6	4.005834000	1.248812000	-0.072662000
6	4.443925000	-1.168670000	-0.000226000
1	2.744639000	-2.476169000	0.038738000
6	4.886451000	0.189352000	-0.035865000
1	4.347001000	2.282421000	-0.114116000
1	5.959931000	0.385747000	-0.036282000
6	-4.295553000	1.418383000	0.114221000
1	-3.692661000	1.986195000	-0.602990000
1	-5.293921000	1.858907000	0.205434000
1	-3.802421000	1.406629000	1.094753000
8	1.723382000	1.921339000	-0.288788000
28	-0.073113000	1.282747000	-0.019874000
6	5.458127000	-2.273468000	0.054743000
1	4.982840000	-3.261058000	0.079880000
1	6.125215000	-2.230221000	-0.819956000
1	6.099116000	-2.172702000	0.943938000
7	-0.704223000	2.811385000	0.466589000
7	-1.052941000	3.926177000	0.495913000
1	-1.148460000	4.526861000	-0.354863000

L-Ni–N–NH_2
Energy: -2479.6655433

6	-4.218649000	-1.985429000	-0.143226000
6	-3.674967000	-0.710790000	-0.117793000
6	-2.251004000	-0.518167000	-0.105687000
6	-1.426387000	-1.695774000	-0.074802000
6	-2.026673000	-2.985743000	-0.098004000
6	-3.397497000	-3.133657000	-0.142081000
1	-5.305711000	-2.076016000	-0.165602000
1	-1.373526000	-3.860199000	-0.083491000
1	-3.849483000	-4.125023000	-0.163424000
8	-4.529839000	0.367572000	-0.187888000
8	-1.798007000	0.708358000	-0.141614000
6	-0.007309000	-1.619459000	-0.040173000
1	0.529743000	-2.573914000	-0.020974000
7	0.693478000	-0.507124000	-0.028639000
6	2.106758000	-0.478077000	0.018201000
6	2.611644000	0.841916000	-0.001483000
6	2.978489000	-1.576621000	0.081774000
6	4.002979000	1.043832000	0.039920000
6	4.361487000	-1.380451000	0.122657000
1	2.589242000	-2.595596000	0.102243000

6	4.853647000	-0.057289000	0.100181000
1	4.395859000	2.061202000	0.024314000
1	5.932979000	0.107318000	0.132001000
6	-4.482407000	1.265485000	0.941255000
1	-3.490067000	1.723894000	1.040227000
1	-5.234988000	2.037195000	0.743636000
1	-4.743628000	0.725354000	1.865448000
8	1.728814000	1.845375000	-0.059021000
28	-0.021960000	1.230272000	-0.098951000
6	5.312443000	-2.550281000	0.189762000
1	4.769559000	-3.504393000	0.207777000
1	5.991420000	-2.565407000	-0.676586000
1	5.943007000	-2.503878000	1.090801000
7	-0.646175000	2.938989000	-0.162202000
7	0.195615000	3.865504000	-0.166881000
1	1.217231000	3.649706000	-0.133792000
1	-0.120262000	4.843139000	-0.202727000

L-Ni–NH –NH
Energy: -2479.6810197

6	-4.189391000	-1.995345000	-0.165590000
6	-3.647004000	-0.720282000	-0.124285000
6	-2.227751000	-0.526538000	-0.109555000
6	-1.395312000	-1.696030000	-0.094700000
6	-1.992581000	-2.986365000	-0.133735000
6	-3.363680000	-3.138975000	-0.179099000
1	-5.276080000	-2.088702000	-0.189292000
1	-1.337456000	-3.859208000	-0.130320000
1	-3.810630000	-4.132133000	-0.213579000
8	-4.492124000	0.368978000	-0.171584000
8	-1.775408000	0.706046000	-0.125885000
6	0.026021000	-1.616438000	-0.054311000
1	0.566850000	-2.568356000	-0.042688000
7	0.724393000	-0.503649000	-0.029520000
6	2.136424000	-0.454063000	0.023286000
6	2.617093000	0.875559000	0.001592000
6	3.022068000	-1.540872000	0.091944000
6	4.006330000	1.098093000	0.045265000
6	4.401029000	-1.322259000	0.135884000
1	2.646823000	-2.565053000	0.114298000
6	4.871812000	0.009636000	0.110790000
1	4.384085000	2.121028000	0.027691000
1	5.948507000	0.190357000	0.145103000
6	-4.520107000	1.151599000	1.039677000
1	-3.518578000	1.525773000	1.293905000
1	-5.193345000	1.993981000	0.844899000
1	-4.914467000	0.548368000	1.872929000
8	1.719364000	1.863783000	-0.060568000
28	-0.010665000	1.205083000	-0.099363000
6	5.371297000	-2.475453000	0.210390000
1	4.845194000	-3.439035000	0.216849000
1	6.062052000	-2.474100000	-0.646635000
1	5.988718000	-2.422168000	1.120158000
7	-0.636319000	2.924564000	-0.198070000
7	-0.046721000	4.024973000	-0.220375000
1	0.973556000	3.809898000	-0.161670000
1	-1.668240000	3.011734000	-0.254754000

L-Ni–NH –NH_2
Energy: -2480.2768416

6	-4.202094000	-2.015659000	-0.174543000
6	-3.657468000	-0.741352000	-0.130327000
6	-2.236917000	-0.548725000	-0.109790000
6	-1.409020000	-1.721186000	-0.091637000
6	-2.007378000	-3.010433000	-0.134937000
6	-3.378942000	-3.161235000	-0.186089000
1	-5.289012000	-2.106688000	-0.201114000
1	-1.353254000	-3.884257000	-0.129695000
1	-3.827743000	-4.153570000	-0.222702000
8	-4.505411000	0.346461000	-0.181025000

8	-1.782438000	0.680816000	-0.122831000
6	0.011989000	-1.639012000	-0.048947000
1	0.554944000	-2.589558000	-0.044592000
7	0.708946000	-0.525011000	-0.016792000
6	2.122505000	-0.488720000	0.026064000
6	2.616999000	0.835437000	0.000109000
6	2.998392000	-1.583799000	0.088764000
6	4.009352000	1.043061000	0.033856000
6	4.380253000	-1.380073000	0.123474000
1	2.613804000	-2.604427000	0.115880000
6	4.865009000	-0.053653000	0.093642000
1	4.397381000	2.062255000	0.013309000
1	5.943768000	0.116173000	0.120479000
6	-4.505075000	1.161138000	1.009407000
1	-3.503070000	1.562215000	1.214670000
1	-5.204352000	1.982852000	0.817105000
1	-4.856204000	0.572999000	1.872427000
8	1.730400000	1.831087000	-0.059621000
28	-0.015130000	1.186925000	-0.069041000
6	5.338011000	-2.544050000	0.196064000
1	4.801508000	-3.501982000	0.193637000
1	6.033840000	-2.545148000	-0.656873000
1	5.950775000	-2.503761000	1.109801000
7	-0.629885000	2.920260000	-0.132024000
7	0.144060000	4.021534000	-0.166639000
1	1.138123000	3.773318000	-0.181881000
1	-1.611055000	3.123916000	-0.339076000
1	-0.141771000	4.766924000	-0.802886000

L-Ni–NH_2 –NH

Energy: -2480.2574405

6	-4.195145000	1.945486000	0.180456000
6	-3.662646000	0.677334000	0.003390000
6	-2.244728000	0.462626000	0.020448000
6	-1.402625000	1.619035000	0.170411000
6	-1.990064000	2.902627000	0.339493000
6	-3.361025000	3.067897000	0.359152000
1	-5.281290000	2.048746000	0.181478000
1	-1.327308000	3.761809000	0.457865000
1	-3.799428000	4.055746000	0.498323000
8	-4.526110000	-0.393083000	-0.107284000
8	-1.803241000	-0.765259000	-0.093622000
6	0.022193000	1.543289000	0.134637000
1	0.556520000	2.498651000	0.175483000
7	0.728371000	0.442157000	0.029627000
6	2.134970000	0.400229000	-0.080120000
6	2.622131000	-0.915704000	-0.298227000
6	3.013378000	1.492858000	0.001420000
6	4.015438000	-1.098774000	-0.431836000
6	4.390480000	1.305949000	-0.130930000
1	2.631226000	2.499696000	0.177283000
6	4.870563000	-0.005019000	-0.350687000
1	4.401224000	-2.105211000	-0.599863000
1	5.946430000	-0.163248000	-0.455617000
6	-4.474031000	-1.080929000	-1.373544000
1	-3.472425000	-1.492370000	-1.559375000
1	-5.206250000	-1.893813000	-1.308945000
1	-4.754763000	-0.396582000	-2.190185000
8	1.752451000	-1.918461000	-0.375745000
28	-0.004429000	-1.275798000	0.004415000
6	5.349089000	2.467108000	-0.035108000
1	4.814250000	3.413733000	0.117521000
1	6.052578000	2.339110000	0.802047000
1	5.953733000	2.564655000	-0.949779000
7	-0.535965000	-3.027039000	0.496619000
7	-0.136421000	-2.523808000	1.726464000
1	0.855970000	-2.794266000	1.808091000
1	-1.550945000	-3.144323000	0.428047000
1	-0.000083000	-3.798810000	0.084522000

L-Ni–NH_2 –NH_2

Energy: -2480.9046566

6	-4.188709000	-2.047583000	-0.123250000
6	-3.644245000	-0.772369000	-0.117037000
6	-2.225495000	-0.576940000	-0.116070000
6	-1.394450000	-1.745454000	-0.077882000
6	-1.991048000	-3.036089000	-0.081680000
6	-3.363106000	-3.191239000	-0.114250000
1	-5.275696000	-2.140686000	-0.136950000
1	-1.335381000	-3.908612000	-0.060682000
1	-3.809543000	-4.185331000	-0.121375000
8	-4.490812000	0.317587000	-0.182907000
8	-1.769495000	0.653512000	-0.161403000
6	0.027401000	-1.657667000	-0.045457000
1	0.574792000	-2.604857000	-0.009480000
7	0.720755000	-0.541262000	-0.054058000
6	2.133475000	-0.496505000	0.003637000
6	2.619677000	0.828799000	-0.071485000
6	3.014200000	-1.582687000	0.124650000
6	4.010357000	1.046561000	-0.031292000
6	4.394410000	-1.368421000	0.166200000
1	2.635022000	-2.603594000	0.191058000
6	4.871740000	-0.041223000	0.085571000
1	4.392662000	2.066451000	-0.091051000
1	5.949149000	0.136220000	0.118097000
6	-4.507061000	1.123338000	1.012265000
1	-3.500466000	1.491498000	1.255732000
1	-5.172905000	1.968899000	0.804948000
1	-4.903368000	0.540696000	1.859415000
8	1.725147000	1.813380000	-0.178698000
28	-0.006866000	1.151977000	-0.180458000
6	5.358299000	-2.522143000	0.298473000
1	4.827542000	-3.482786000	0.330136000
1	6.064186000	-2.554788000	-0.545570000
1	5.960088000	-2.439825000	1.216724000
7	-0.667685000	2.975196000	-0.366965000
7	0.040307000	3.959804000	0.428069000
1	1.019466000	3.649713000	0.406910000
1	-0.646402000	3.201759000	-1.369442000
1	-1.649067000	2.956015000	-0.075295000
1	-0.002877000	4.859596000	-0.059965000

LH-Ni–NH_2 –NH_2

Energy: -2481.4631306

6	-4.318721000	-1.958858000	-0.141407000
6	-3.777315000	-0.686360000	-0.069885000
6	-2.355192000	-0.458486000	-0.096808000
6	-1.512254000	-1.636914000	-0.176489000
6	-2.116052000	-2.925194000	-0.251566000
6	-3.486128000	-3.094949000	-0.242624000
1	-5.405403000	-2.059277000	-0.119436000
1	-1.456345000	-3.793747000	-0.320215000
1	-3.924655000	-4.091248000	-0.301984000
8	-4.645325000	0.393612000	-0.038012000
8	-1.918344000	0.768881000	-0.064222000
6	-0.083808000	-1.599908000	-0.216570000
1	0.413342000	-2.576323000	-0.296898000
7	0.654553000	-0.506229000	-0.187026000
6	2.062393000	-0.564992000	-0.122844000
6	2.753226000	0.642207000	-0.384095000
6	2.815944000	-1.690001000	0.257457000
6	4.137156000	0.716814000	-0.264143000
6	4.210348000	-1.634348000	0.376289000
1	2.303879000	-2.620968000	0.504850000
6	4.861873000	-0.416908000	0.117964000
1	4.642012000	1.661343000	-0.472607000
1	5.946524000	-0.352098000	0.220202000
6	-4.591011000	1.164319000	1.176570000
1	-3.582106000	1.567230000	1.340828000

1	-5.307907000	1.985044000	1.053019000
1	-4.891195000	0.543302000	2.037152000
8	1.983953000	1.716222000	-0.800432000
28	-0.059657000	1.239782000	-0.254700000
6	4.996183000	-2.863018000	0.763667000
1	4.389383000	-3.554160000	1.364125000
1	5.333603000	-3.413570000	-0.128966000
1	5.892489000	-2.598968000	1.341381000
7	-0.241876000	3.261165000	-0.055956000
7	0.976292000	3.758494000	0.586708000
1	2.076595000	2.549385000	-0.247448000
1	-0.257514000	3.667529000	-0.996571000
1	-1.080066000	3.606087000	0.425356000
1	0.955497000	4.783051000	0.646341000
1	0.957342000	3.399359000	1.544636000

L-Ni–NH_3 –NH_2
Energy: -2481.4523169

6	-4.423931000	-1.589863000	-0.477258000
6	-3.826060000	-0.400281000	-0.092456000
6	-2.401485000	-0.277437000	0.040140000
6	-1.611770000	-1.464039000	-0.217023000
6	-2.272634000	-2.664627000	-0.603245000
6	-3.644985000	-2.735216000	-0.743105000
1	-5.511015000	-1.614052000	-0.569478000
1	-1.656230000	-3.546239000	-0.794394000
1	-4.125903000	-3.665972000	-1.044365000
8	-4.632859000	0.708884000	0.095365000
8	-1.915892000	0.896215000	0.374367000
6	-0.181178000	-1.521083000	-0.125753000
1	0.273771000	-2.501192000	-0.328423000
7	0.586597000	-0.498537000	0.172020000
6	1.983061000	-0.507281000	0.268999000
6	2.522349000	0.777851000	0.590862000
6	2.831526000	-1.612278000	0.082224000
6	3.923889000	0.896470000	0.699569000
6	4.217434000	-1.485199000	0.200773000
1	2.406421000	-2.589759000	-0.156814000
6	4.745358000	-0.212492000	0.510087000
1	4.348795000	1.872933000	0.939583000
1	5.827694000	-0.095721000	0.605059000
6	-4.669222000	1.198767000	1.450033000
1	-3.667243000	1.494063000	1.789891000
1	-5.334094000	2.070566000	1.443038000
1	-5.081454000	0.428817000	2.122741000
8	1.701443000	1.820589000	0.749999000
28	-0.113629000	1.233854000	0.541075000
6	5.130884000	-2.672682000	0.016327000
1	4.568989000	-3.561280000	-0.301207000
1	5.904469000	-2.473386000	-0.741035000
1	5.656113000	-2.926051000	0.950699000
7	0.433279000	2.181691000	-2.197214000
7	1.812924000	2.617866000	-2.032840000
1	1.945554000	2.591003000	-0.999788000
1	0.337008000	1.510020000	-2.967158000
1	-0.154645000	2.996114000	-2.409424000
1	2.391206000	1.851332000	-2.389373000
1	0.061633000	1.714602000	-1.252286000

LH-Ni–NH_2 + NH_3
Energy: -2482.0906385

6	-4.630951000	-1.481062000	0.001884000
6	-4.006919000	-0.244677000	0.066856000
6	-2.581564000	-0.137499000	-0.056682000
6	-1.837673000	-1.356916000	-0.209458000
6	-2.515012000	-2.605193000	-0.266237000
6	-3.891067000	-2.670662000	-0.172544000
1	-5.718474000	-1.508549000	0.087682000
1	-1.922167000	-3.513469000	-0.390040000
1	-4.407035000	-3.629255000	-0.220893000

8	-4.790458000	0.885789000	0.170542000
8	-2.015373000	1.038161000	-0.041347000
6	-0.419012000	-1.348360000	-0.322834000
1	0.076749000	-2.321931000	-0.411887000
7	0.366246000	-0.289349000	-0.338999000
6	1.777325000	-0.514335000	-0.337205000
6	2.572829000	-0.082763000	-1.417755000
6	2.378637000	-1.151630000	0.752722000
6	3.955498000	-0.278916000	-1.360474000
6	3.763631000	-1.365126000	0.815438000
1	1.739130000	-1.456001000	1.583405000
6	4.540982000	-0.909281000	-0.258881000
1	4.577854000	0.062123000	-2.190937000
1	5.623590000	-1.045285000	-0.237480000
6	-4.566656000	1.675966000	1.356737000
1	-3.532901000	2.043712000	1.398811000
1	-5.262397000	2.520304000	1.293939000
1	-4.790169000	1.080909000	2.256892000
8	1.949229000	0.512766000	-2.479257000
28	-0.222521000	1.425525000	-0.190350000
6	4.384746000	-2.067462000	1.996531000
1	3.920256000	-1.751435000	2.941058000
1	4.257921000	-3.158907000	1.921319000
1	5.461696000	-1.863223000	2.057819000
7	1.105033000	2.611047000	-0.235645000
7	3.435969000	2.056241000	1.772242000
1	2.620226000	0.751235000	-3.142787000
1	1.564791000	2.779495000	-1.138180000
1	1.860778000	2.603971000	0.473050000
1	3.137668000	1.873105000	2.732972000
1	3.655750000	1.142169000	1.365167000
1	4.320635000	2.564533000	1.838626000

L-Ni Monomer
Energy: -2368.9147458

6	4.261304000	1.575008000	-0.125797000
6	3.690969000	0.310252000	-0.137208000
6	2.269921000	0.154816000	-0.116682000
6	1.461832000	1.341226000	-0.047744000
6	2.088487000	2.617755000	-0.033484000
6	3.463197000	2.736532000	-0.081175000
1	5.349564000	1.644053000	-0.154375000
1	1.456498000	3.505936000	0.012314000
1	3.934403000	3.718962000	-0.073931000
8	4.514128000	-0.789485000	-0.247504000
8	1.756365000	-1.053148000	-0.176883000
6	0.039992000	1.280601000	-0.010990000
1	-0.493579000	2.234105000	0.041225000
7	-0.691484000	0.186743000	-0.034770000
6	-2.107495000	0.141504000	0.009134000
6	-2.583253000	-1.187761000	-0.054165000
6	-2.984303000	1.231907000	0.103471000
6	-3.973391000	-1.409389000	-0.024169000
6	-4.363636000	1.010829000	0.132926000
1	-2.606399000	2.253814000	0.155125000
6	-4.835392000	-0.320083000	0.067551000
1	-4.354030000	-2.430161000	-0.073344000
1	-5.912751000	-0.498508000	0.090137000
6	4.483027000	-1.687176000	0.881718000
1	3.478289000	-2.105894000	1.029376000
1	5.190949000	-2.490584000	0.649763000
1	4.806637000	-1.161401000	1.793972000
8	-1.674391000	-2.161178000	-0.140345000
28	0.019478000	-1.467361000	-0.152262000
6	-5.334284000	2.161837000	0.232779000
1	-4.808443000	3.124853000	0.268647000
1	-6.019630000	2.183502000	-0.628282000
1	-5.957167000	2.083574000	1.136983000

N_2

Energy: -109.5753301

7	0.000000000	0.000000000	0.551431000
7	0.000000000	0.000000000	-0.551431000

N_2-H
Energy: -110.0755164

7	0.049332000	0.491555000	0.000000000
7	0.049332000	-0.687770000	0.000000000
1	-0.690647000	1.373509000	0.000000000

NH_3
Energy: -56.5920012

7	-0.000017000	0.000037000	-0.120718000
1	0.749209000	0.569004000	0.281693000
1	-0.867460000	0.364076000	0.281736000
1	0.118372000	-0.933341000	0.281597000

L-Ni Monomer Radical anion
Energy: -2369.0406383

6	4.266948000	1.609505000	-0.122092000
6	3.703455000	0.342372000	-0.133923000
6	2.281678000	0.137759000	-0.127450000
6	1.448274000	1.324864000	-0.059714000
6	2.073751000	2.603864000	-0.048382000
6	3.447151000	2.757292000	-0.088438000
1	5.355072000	1.691956000	-0.141519000
1	1.426580000	3.484155000	-0.009805000
1	3.895883000	3.751339000	-0.083130000
8	4.558269000	-0.747161000	-0.225305000
8	1.835066000	-1.094336000	-0.195325000
6	0.013680000	1.308367000	-0.022044000
1	-0.475809000	2.292870000	0.024112000
7	-0.717267000	0.214047000	-0.040272000
6	-2.111282000	0.148944000	0.005340000
6	-2.599908000	-1.202778000	-0.050554000
6	-3.003969000	1.231057000	0.098836000
6	-4.003350000	-1.387405000	-0.010321000
6	-4.386548000	1.030282000	0.138391000
1	-2.615391000	2.251868000	0.143595000
6	-4.866465000	-0.297635000	0.081213000
1	-4.394138000	-2.406508000	-0.053388000
1	-5.945425000	-0.473168000	0.110839000
6	4.522253000	-1.628786000	0.911533000
1	3.517152000	-2.049145000	1.053096000
1	5.238749000	-2.432165000	0.700659000
1	4.834436000	-1.090637000	1.822568000
8	-1.745799000	-2.206412000	-0.136341000
28	0.041776000	-1.523779000	-0.161560000
6	-5.345214000	2.192720000	0.241873000
1	-4.805896000	3.149633000	0.270372000
1	-6.039181000	2.226525000	-0.613292000
1	-5.963919000	2.131487000	1.151630000